Perturbing relativistic, magnetized jets: instabilities, and the interaction with the environment

Nektarios Vlahakis
University of Athens

Outline

- relativistic jet properties
- linear stability analysis and resulting growth rates
- “body” and “surface” interactions – the Riemann problem

Astrophysical jet examples

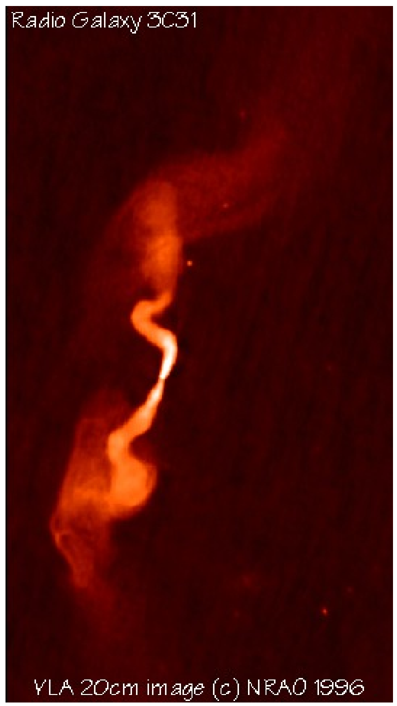

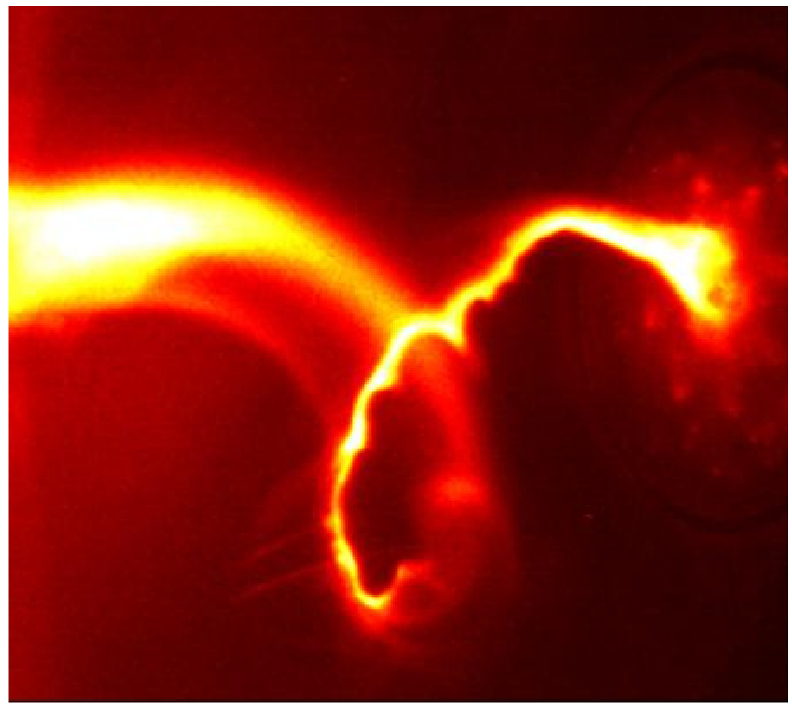

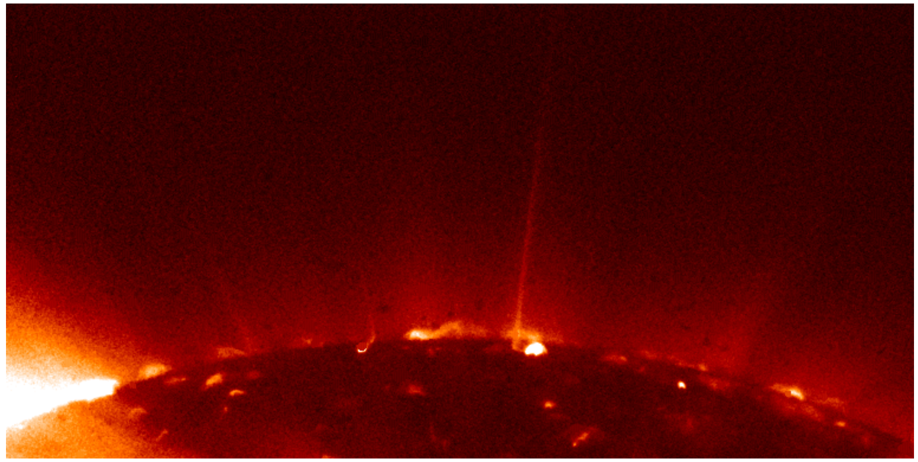

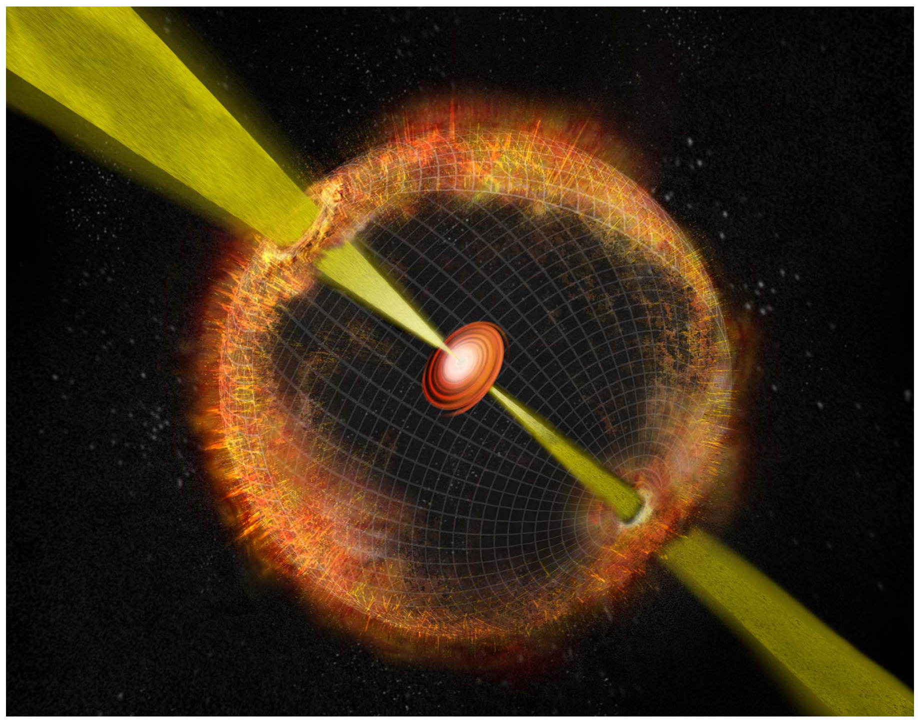

Relativistic jet models: Why magnetic fields

- Hydrodynamics give Lorentz factors $\gamma \sim k_{\rm B} T_i / m_p c^2$ – need very high initial temperatures T_i to explain observations

- Hydrodynamic acceleration is a fast process (saturates at distances where gravity is still important) while observations imply pc-scale acceleration

- Magnetic fields tap the rotational energy of central object or accretion disk

- “Clean” energy extraction – makes high $\gamma = \dot{\mathcal{E}} / \dot{M} c^2$ possible

- Radiation through shocks (particle acceleration and synchrotron/inverse Compton mechanisms) or magnetic reconnection

Polarization

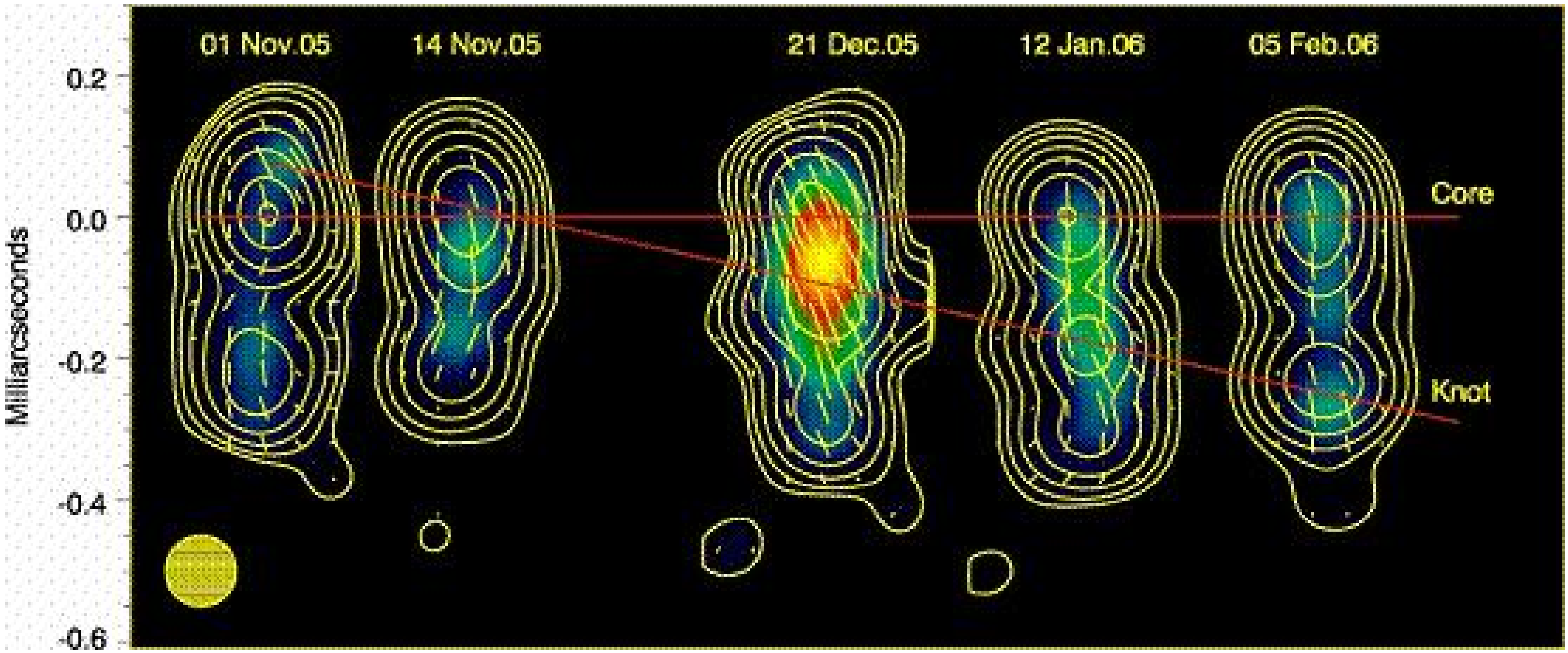

(Marscher et al 2008, Nature)

observed $\boldsymbol{E}_{\rm rad} \perp \boldsymbol{B}_{\perp \rm los}$
(modified by Faraday rotation and relativistic effects)

Faraday RM gradients across the jet

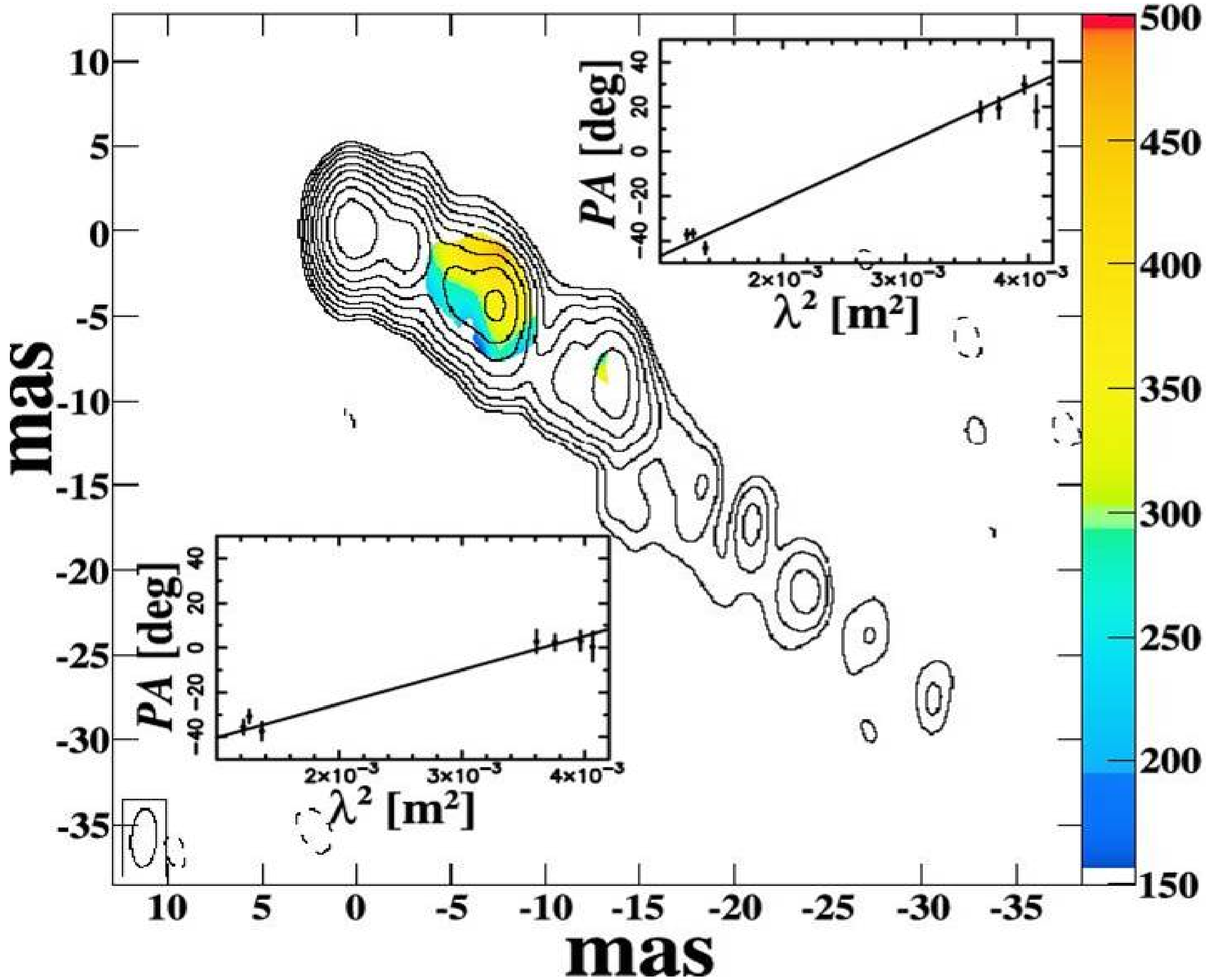

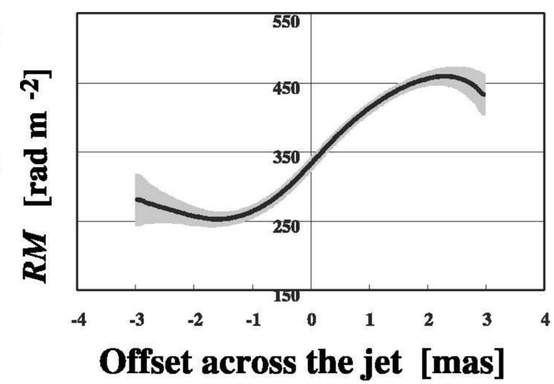

(Asada et al)

helical field surrounding the emitting region (Gabuzda)

What magnetic fields can do

- ⋆ extract energy (Poynting flux)
- ⋆ extract angular momentum
- ⋆ transfer energy and angular momentum to matter
- ⋆ explain relatively large-scale acceleration
- ⋆ self-collimation
- ⋆ synchrotron emission
- ⋆ polarization and RM maps

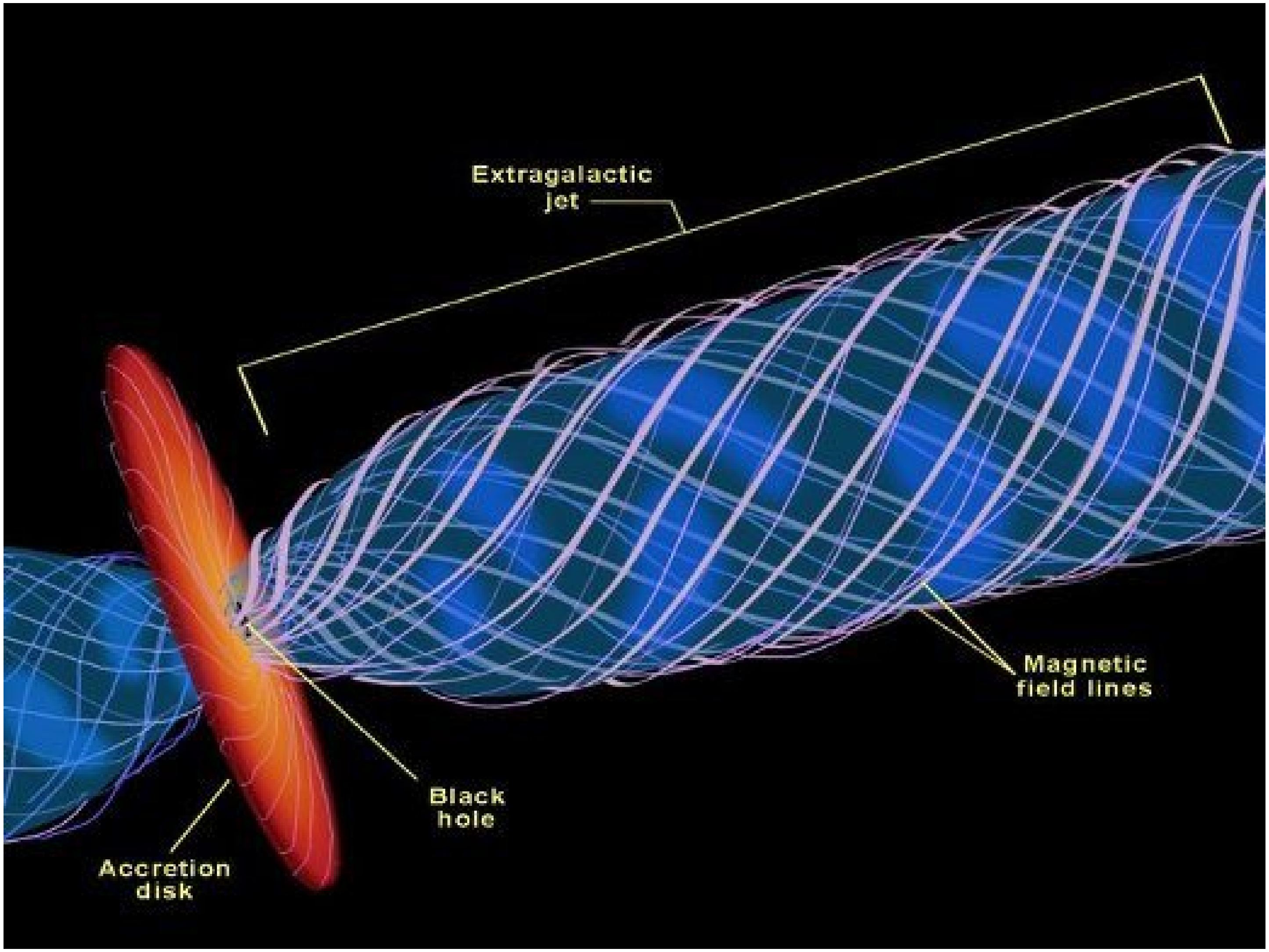

B field from advection, or dynamo, or cosmic battery

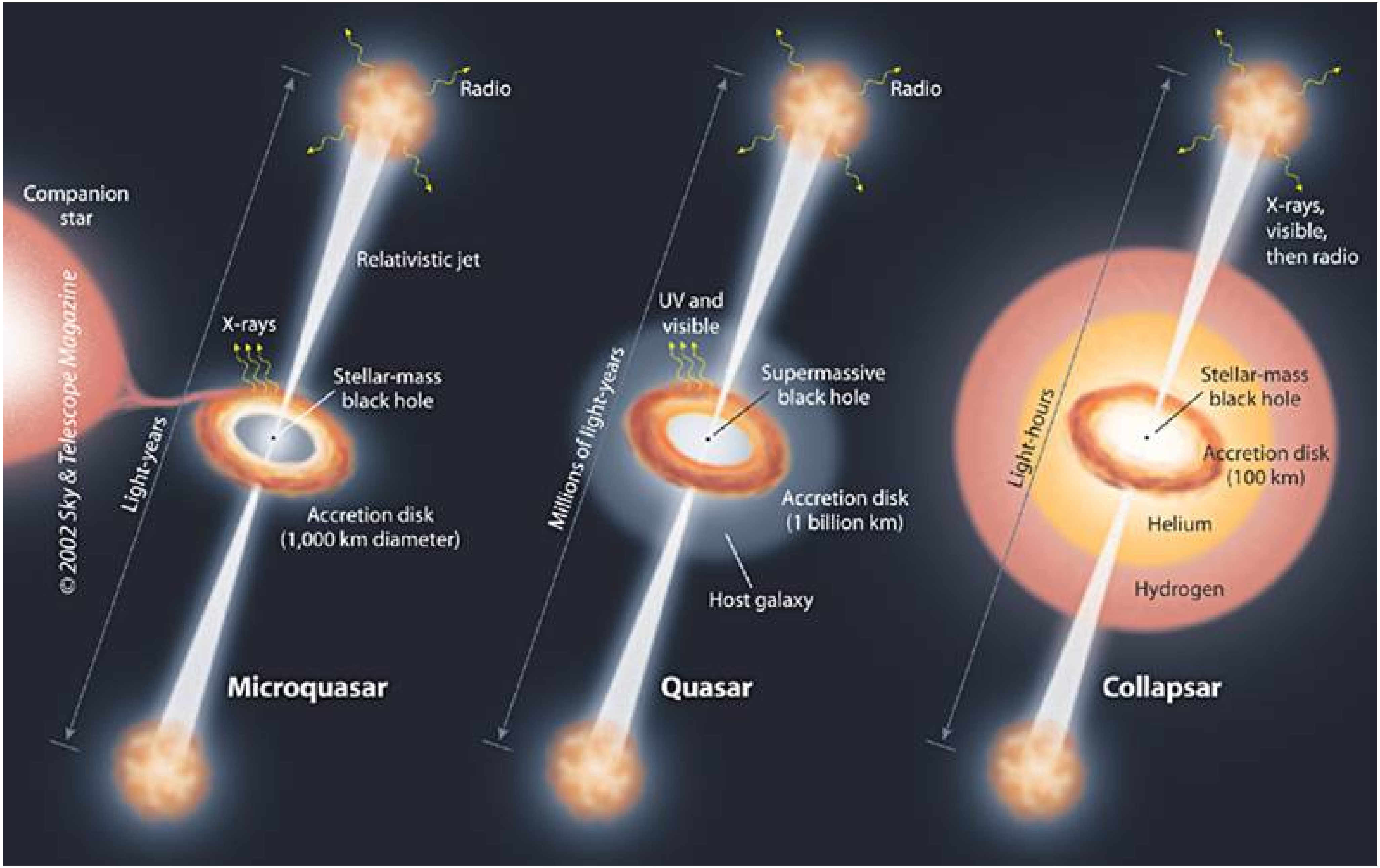

Radio
Radio
Companion star
Relativistic jet
X-rays, visible, then radio
UV and visible
X-rays
Stellar-mass black hole
Supermassive black hole
Stellar-mass black hole
© 2002 Sky & Telescope Magazine
Light-years
Millions of light-years
Light-hours
Accretion disk (100 km)
Accretion disk (1 billion km)
Accretion disk (1,000 km diameter)
Helium
Host galaxy
Hydrogen
Microquasar
Quasar
Collapsar

A unipolar inductor

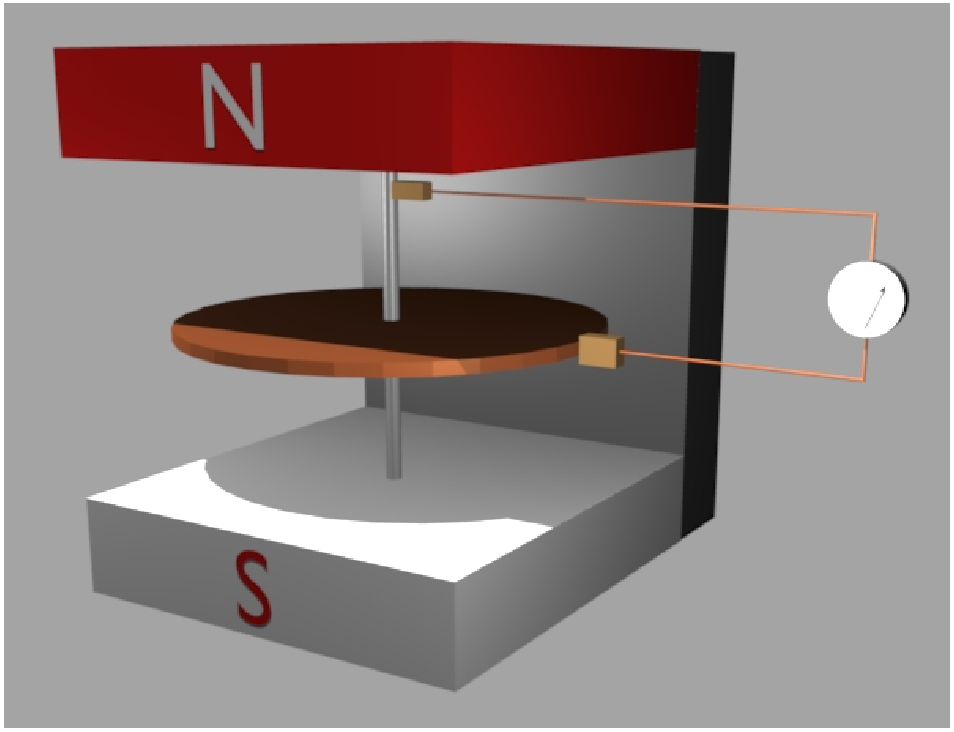

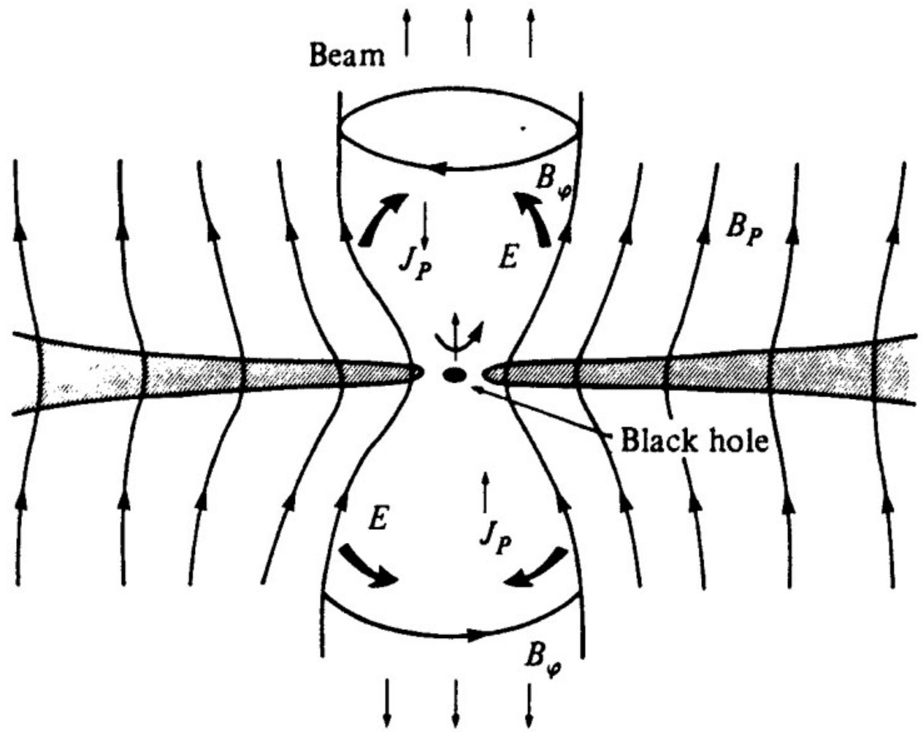

current $\leftrightarrow B_\phi$

Poynting flux $\frac{c}{4\pi}EB_\phi$ is extracted (angular momentum as well)

The Faraday disk could be the rotating accretion disk, or the frame dragging if energy is extracted from the ergosphere of a rotating black hole (Blandford & Znajek mechanism - the electromagnetic analogue of the Penrose mechanism)

Acceleration efficiency

- Analytical steady-state self-similar models
(radial self-similar Blandford & Payne, Li, Chiueh & Begelman, Contopoulos & Lovelace, Vlahakis & Königl, and meridionally self-similar Sauty & Tsinganos, Vlahakis & Tsinganos)
$\rightarrow$ efficient conversion of Poynting to kinetic energy flux

- Verified and extended by axisymmetric numerical simulations (Komissarov, Vlahakis & Königl, Tchekhovskoy, McKinney & Narayan)

- role of environment: $\gamma \gtrsim 100$ achievable only for confined outflows (unconfined remain Poynting dominated)

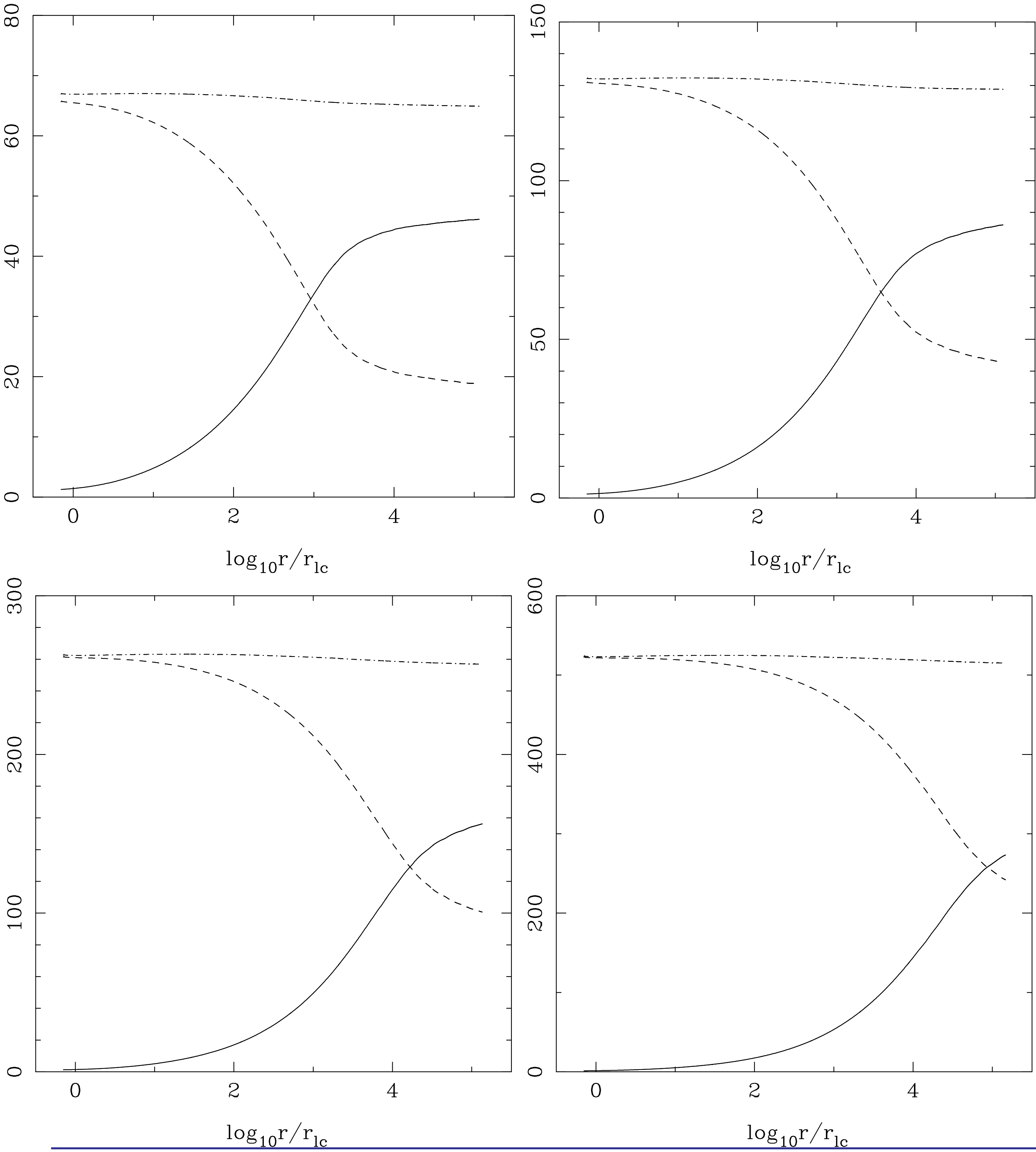

energy flux ratios:

$$\gamma = \frac{\text{kinetic}}{\text{rest mass}}$$

$$\gamma\sigma = \frac{\text{Poynting}}{\text{rest mass}}$$

$$(\sigma = \frac{\text{Poynting}}{\text{kinetic}})$$

$$\mu = \gamma + \gamma\sigma$$

γ (increasing),

$\gamma\sigma$ (decreasing),

and μ (constant)

efficiency $> 50\%$

Magnetohydrodynamics

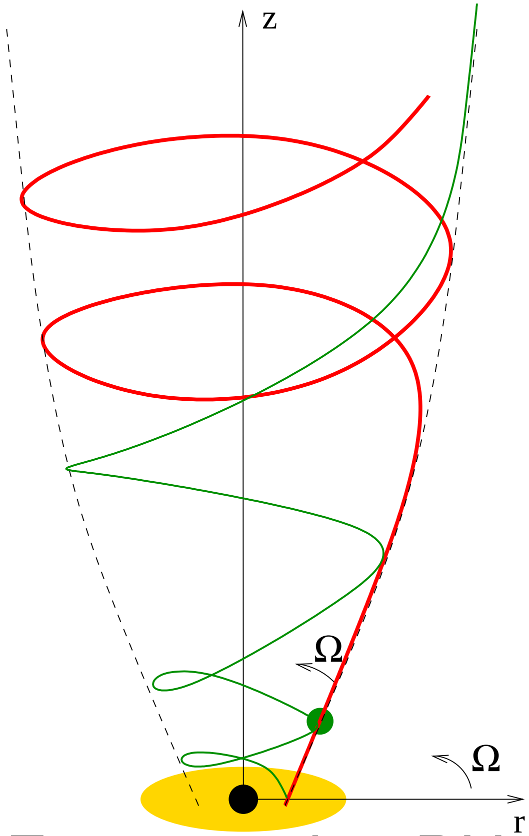

- successfully explain the main characteristics

- At small distances $V_\phi \gg V_p$, $|B_\phi| \ll B_p$. At large distances $V_\phi \ll V_p$, $|B_\phi| \gg B_p$.

- From Ferraro's law $V_\phi = r\Omega + V_p B_\phi / B_p$, where Ω integral of motion = rotation at base, we get $-B_\phi/B_p \approx r\Omega/V_p$, or, $-B_\phi/B_p \approx r/r_{\rm LC}$.

For a rotating BH-jet

$$\frac{|B_\phi|}{B_z} \approx 150 \left(\frac{r_j}{10^{16}{\rm cm}}\right) \left(\frac{r_{\rm LC}}{4GM/c^2}\right) \left(\frac{M}{10^8 M_\odot}\right)^{-1}$$

For a disk-jet $\dfrac{|B_\phi|}{B_z} \approx 20 \left(\dfrac{r_j}{10^{16}{\rm cm}}\right) \left(\dfrac{r_0}{10GM/c^2}\right)^{-3/2} \left(\dfrac{M}{10^8 M_\odot}\right)^{-1}$

Strong B_ϕ induces current-driven instabilities (Kruskal-Shafranov)

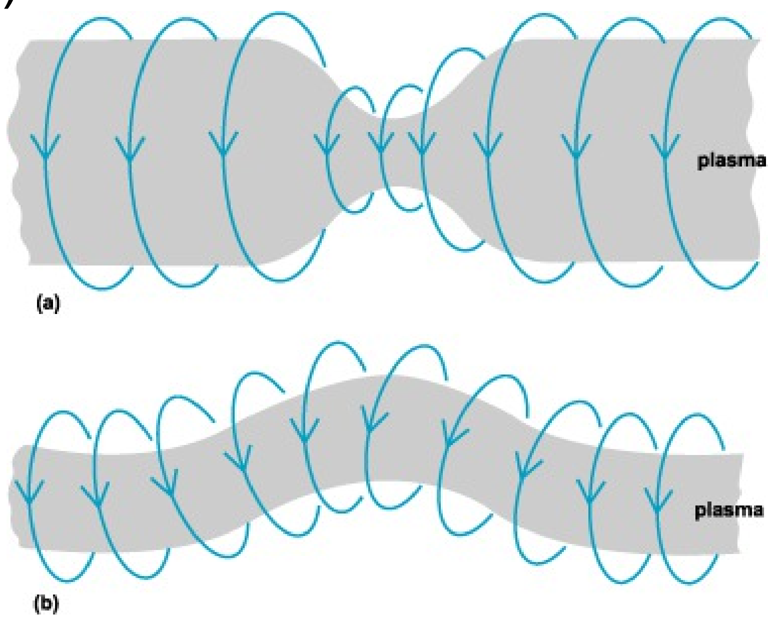

Interaction with the environment $\rightarrow$ Kelvin-Helmholtz instabilities

Stability of axisymmetric solutions (analytical or numerical)? Role of B_z? of inertia?

Relation with observations? (knot structure, jet bending, shocks, polarization degree, reconnection)

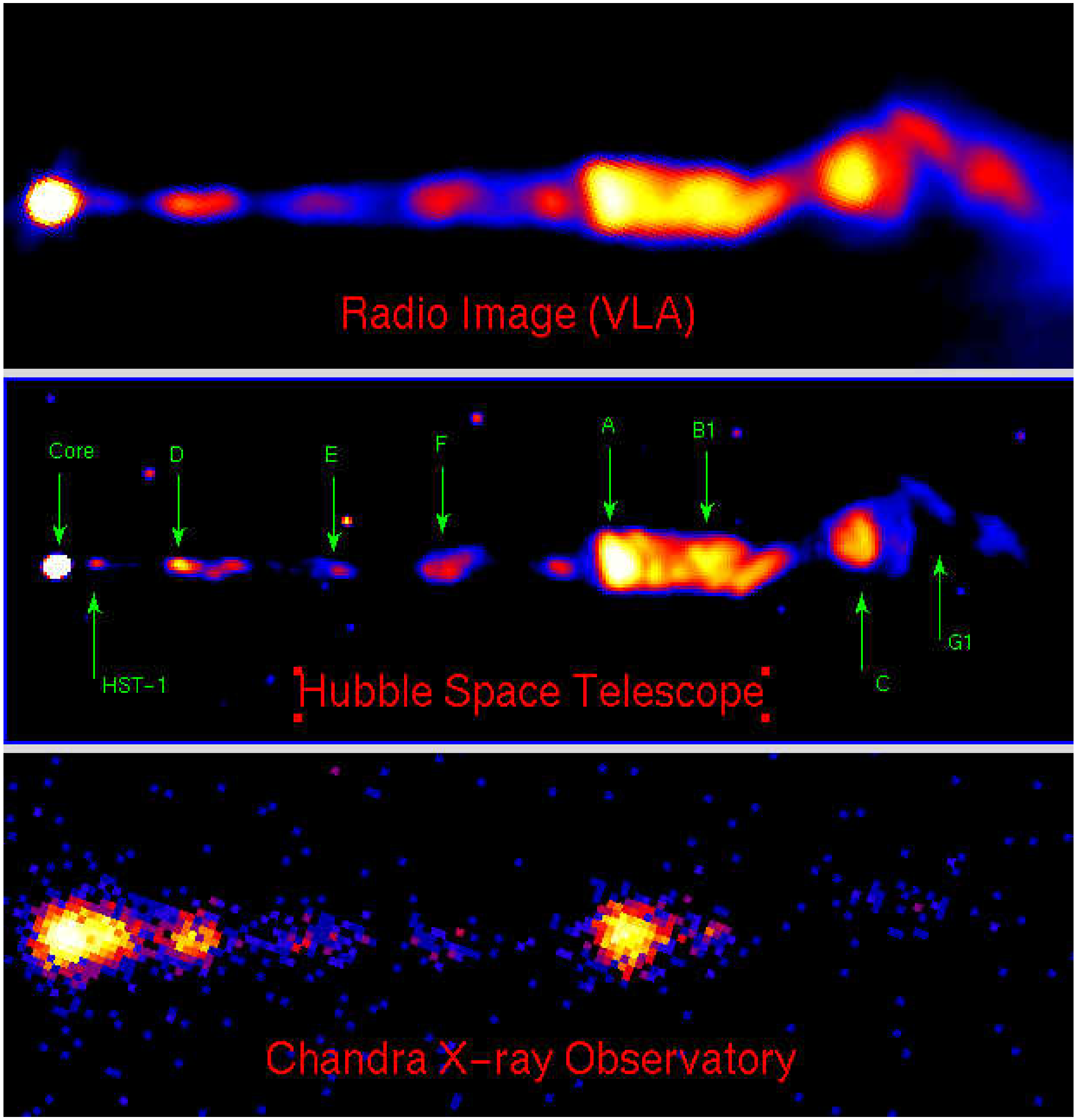
Radio Image (VLA)
Core
D
E
F
A
B1
HST-1
C
G1
Hubble Space Telescope
Chandra X-ray Observatory

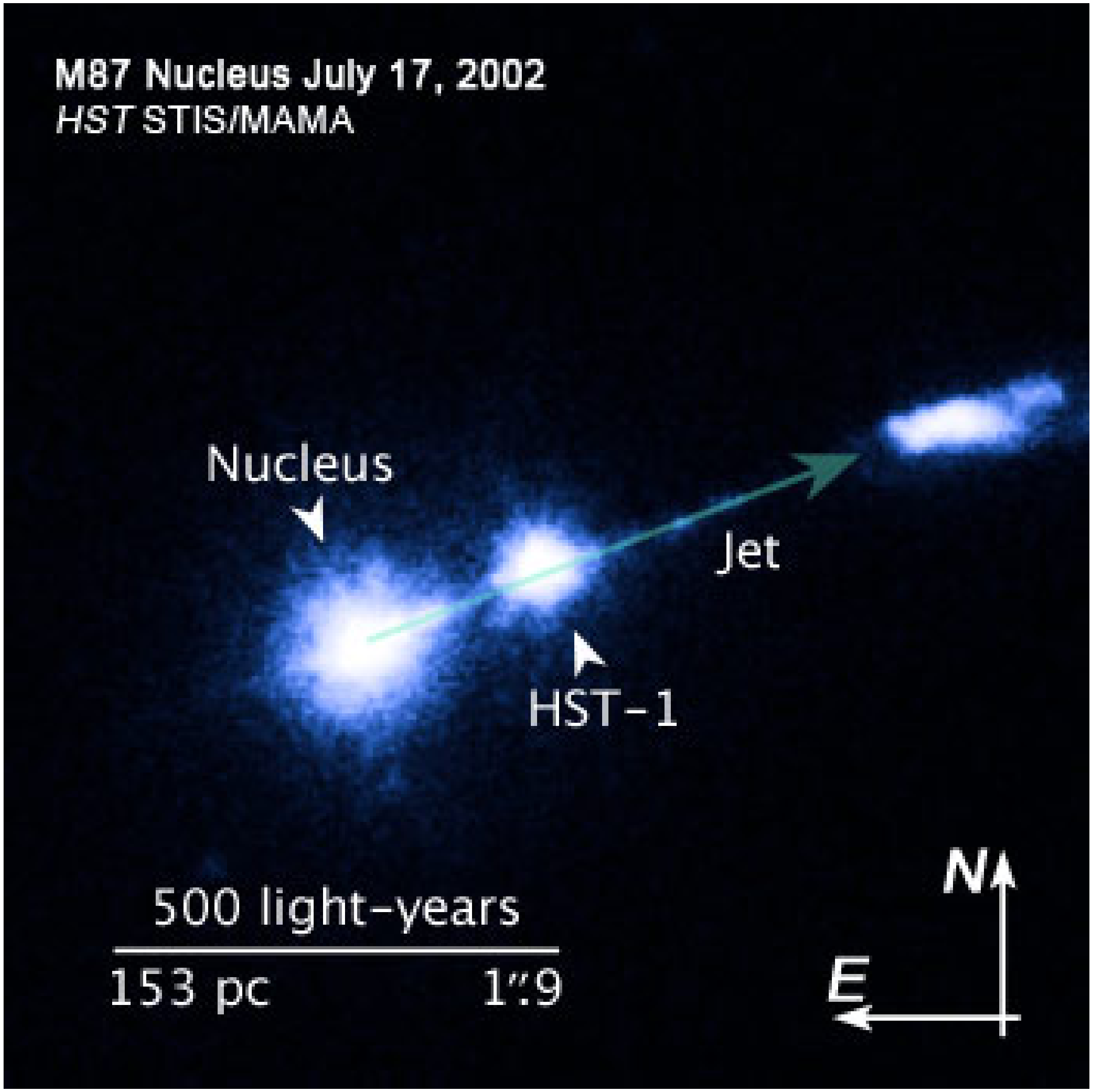
M87 Nucleus July 17, 2002
HST STIS/MAMA
Nucleus
Jet
HST-1
500 light-years
153 pc
1″.9
N
E

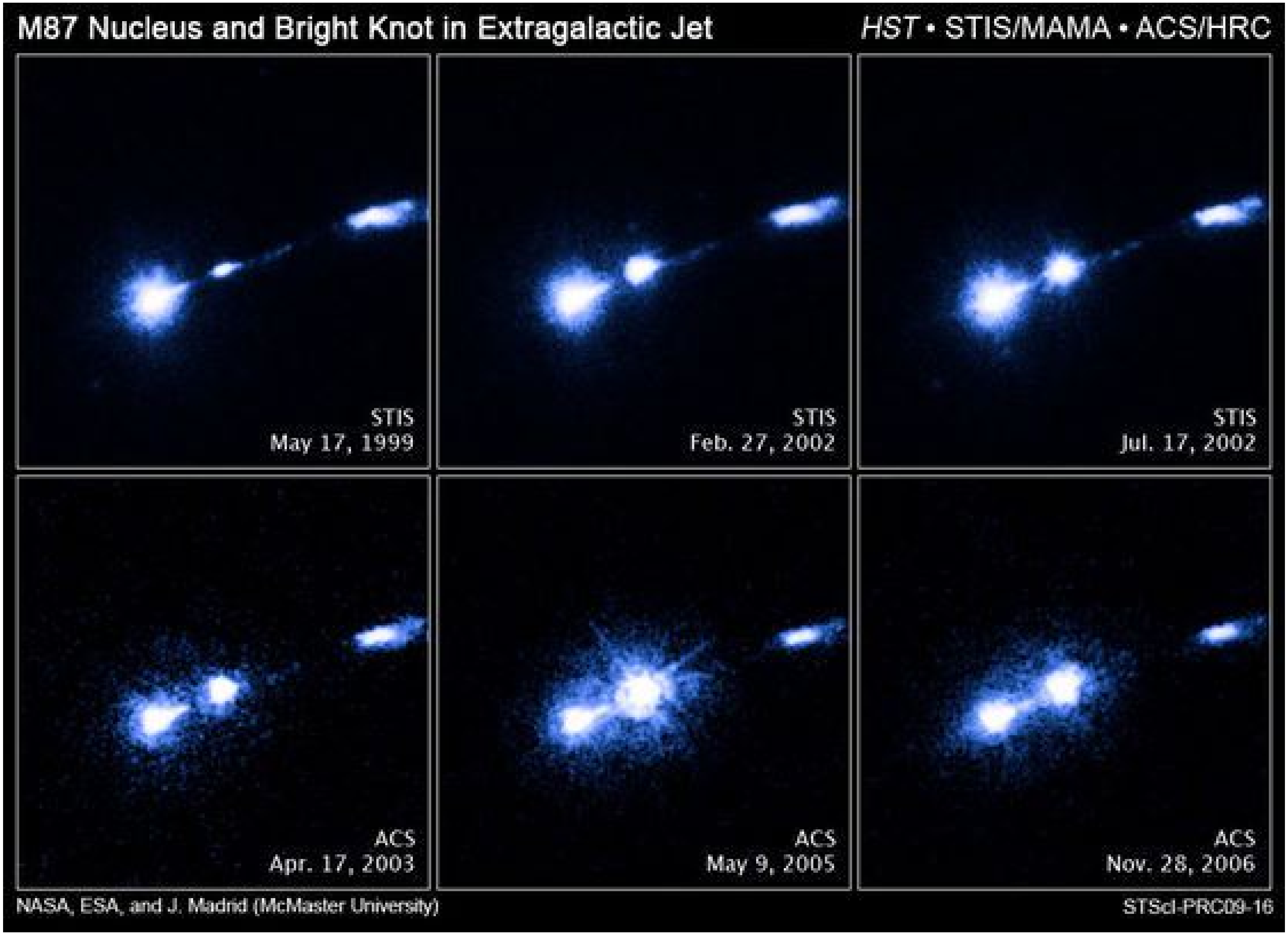
M87 Nucleus and Bright Knot in Extragalactic Jet
HST • STIS/MAMA • ACS/HRC
STIS
May 17, 1999
STIS
Feb. 27, 2002
STIS
Jul. 17, 2002
ACS
Apr. 17, 2003
ACS
May 9, 2005
ACS
Nov. 28, 2006
NASA, ESA, and J. Madrid (McMaster University)
STScI-PRC09-16

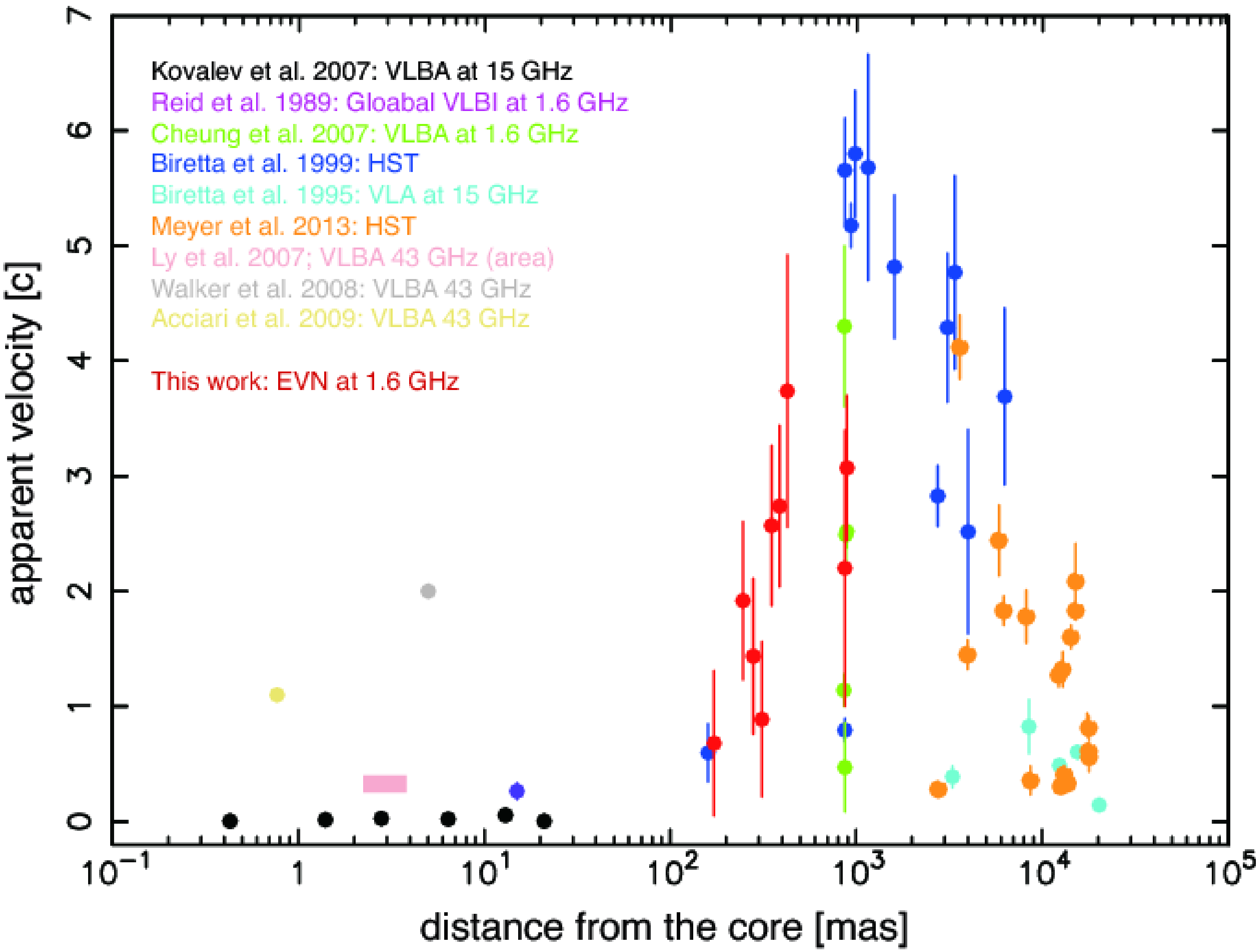
Kovalev et al. 2007: VLBA at 15 GHz
Reid et al. 1989: Gloabal VLBI at 1.6 GHz
Cheung et al. 2007: VLBA at 1.6 GHz
Biretta et al. 1999: HST
Biretta et al. 1995: VLA at 15 GHz
Meyer et al. 2013: HST
Ly et al. 2007; VLBA 43 GHz (area)
Walker et al. 2008: VLBA 43 GHz
Acciari et al. 2009: VLBA 43 GHz
This work: EVN at 1.6 GHz
apparent velocity [c]
distance from the core [mas]

Asada+2013

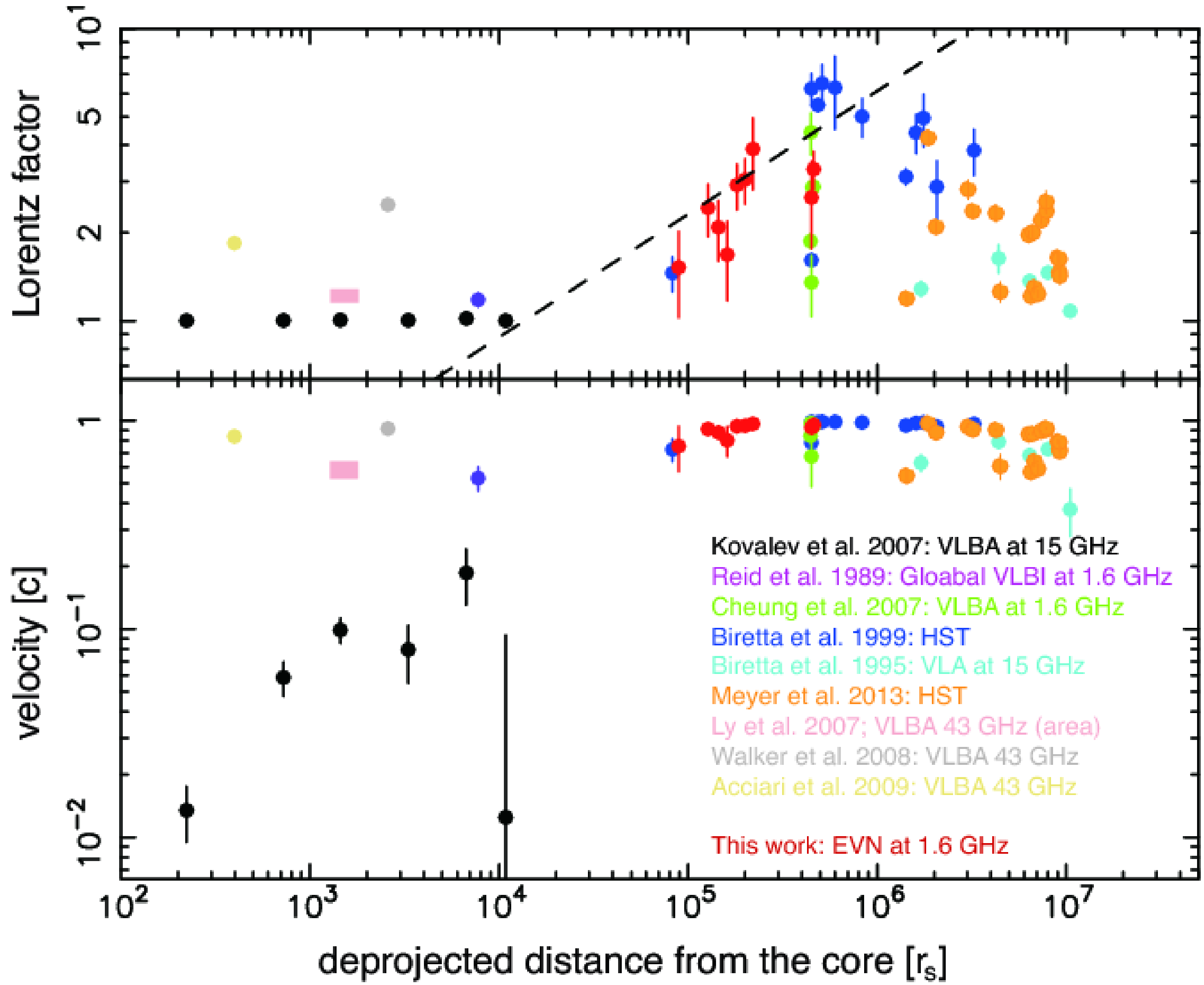

Lorentz factor
velocity [c]
deprojected distance from the core [r_s]
Kovalev et al. 2007: VLBA at 15 GHz
Reid et al. 1989: Gloabal VLBI at 1.6 GHz
Cheung et al. 2007: VLBA at 1.6 GHz
Biretta et al. 1999: HST
Biretta et al. 1995: VLA at 15 GHz
Meyer et al. 2013: HST
Ly et al. 2007; VLBA 43 GHz (area)
Walker et al. 2008: VLBA 43 GHz
Acciari et al. 2009: VLBA 43 GHz
This work: EVN at 1.6 GHz

(Asada & Nakamura 2011)

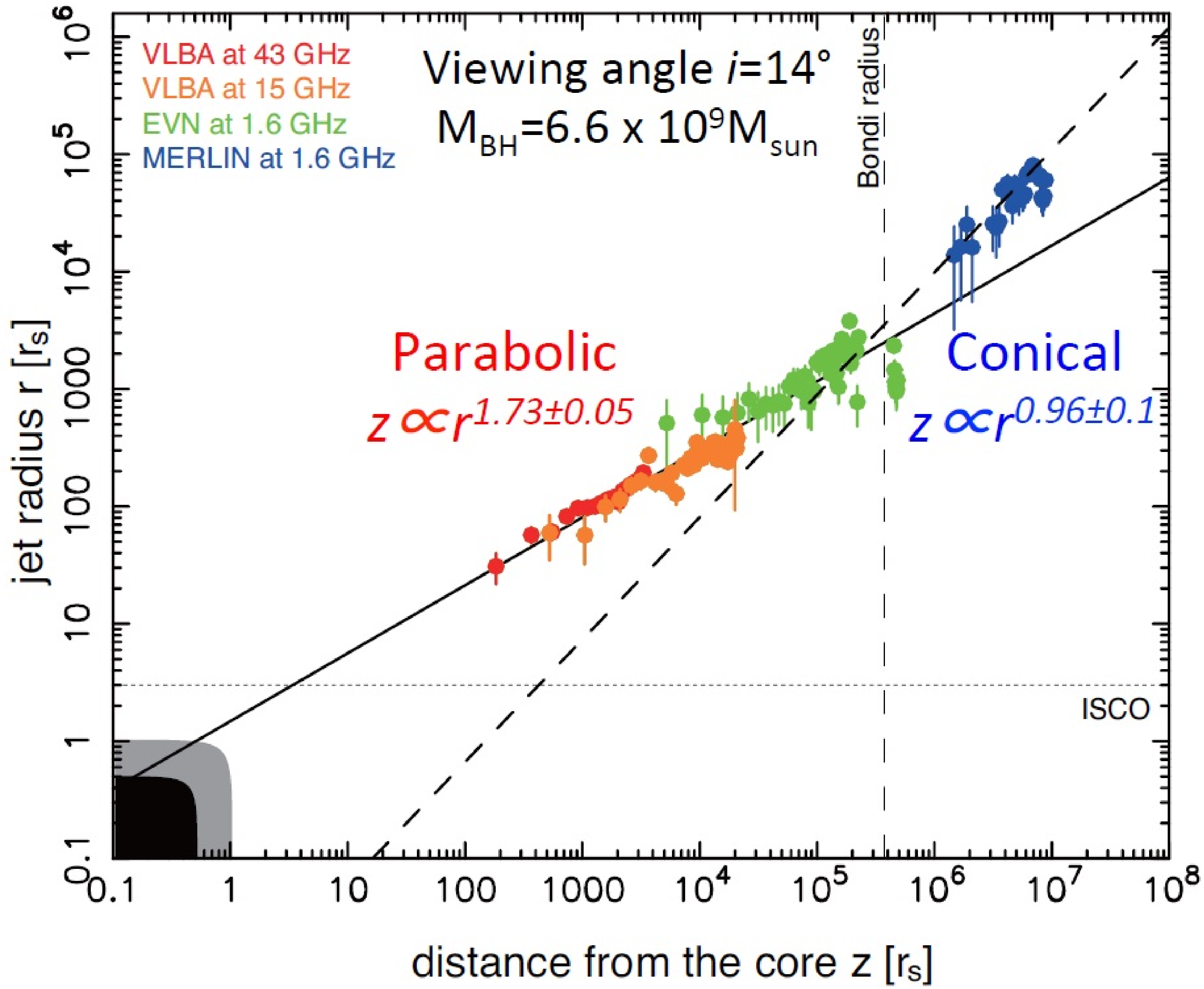

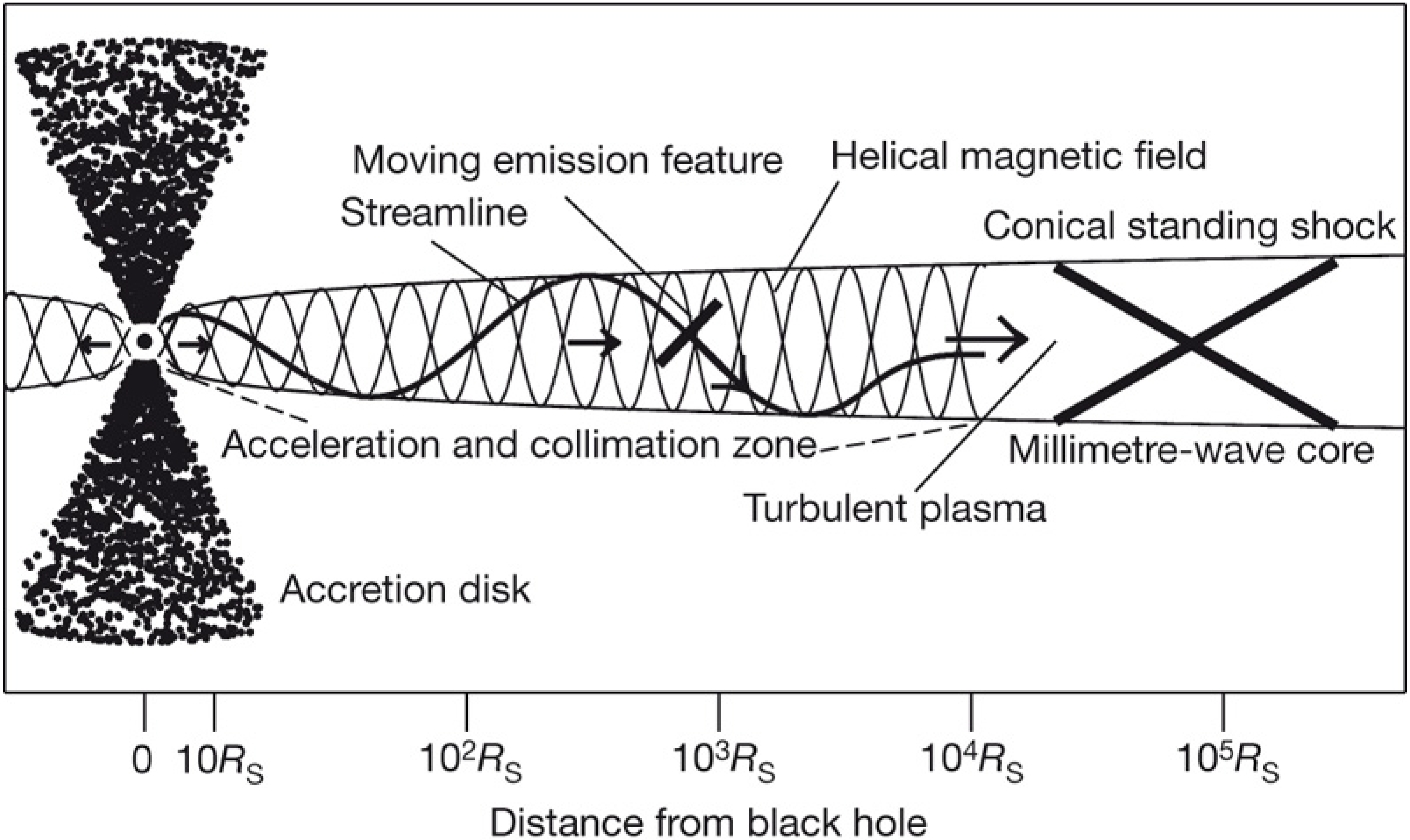

Marscher+ 2008, Nature

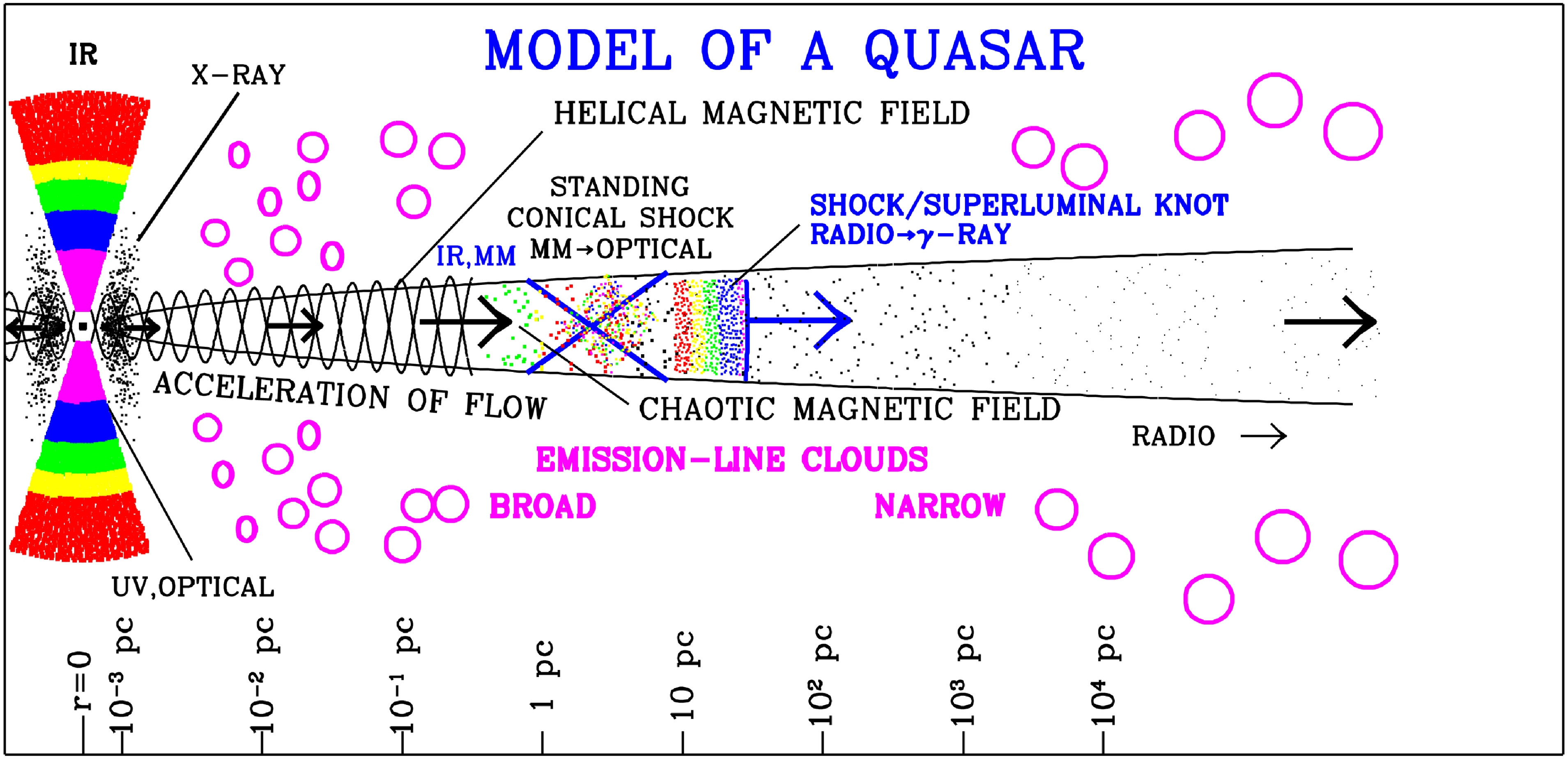
MODEL OF A QUASAR
IR
X-RAY
HELICAL MAGNETIC FIELD
STANDING
CONICAL SHOCK
MM→OPTICAL
IR,MM
SHOCK/SUPERLUMINAL KNOT
RADIO→γ-RAY
ACCELERATION OF FLOW
CHAOTIC MAGNETIC FIELD
RADIO →
EMISSION-LINE CLOUDS
BROAD
NARROW
UV,OPTICAL
r=0
10⁻³ pc
10⁻² pc
10⁻¹ pc
1 pc
10 pc
10² pc
10³ pc
10⁴ pc

Stability analysis

- Why astrophysical jets are stable? (contrary to lab jets)

- 3D relativistic MHD simulations hard to cover the full jet range (one needs to simulate formation and propagation zone + environment)

interesting results for the jet-formation region (McKinney & Blandford, Tchekhovskoy, Narayan & McKinney)

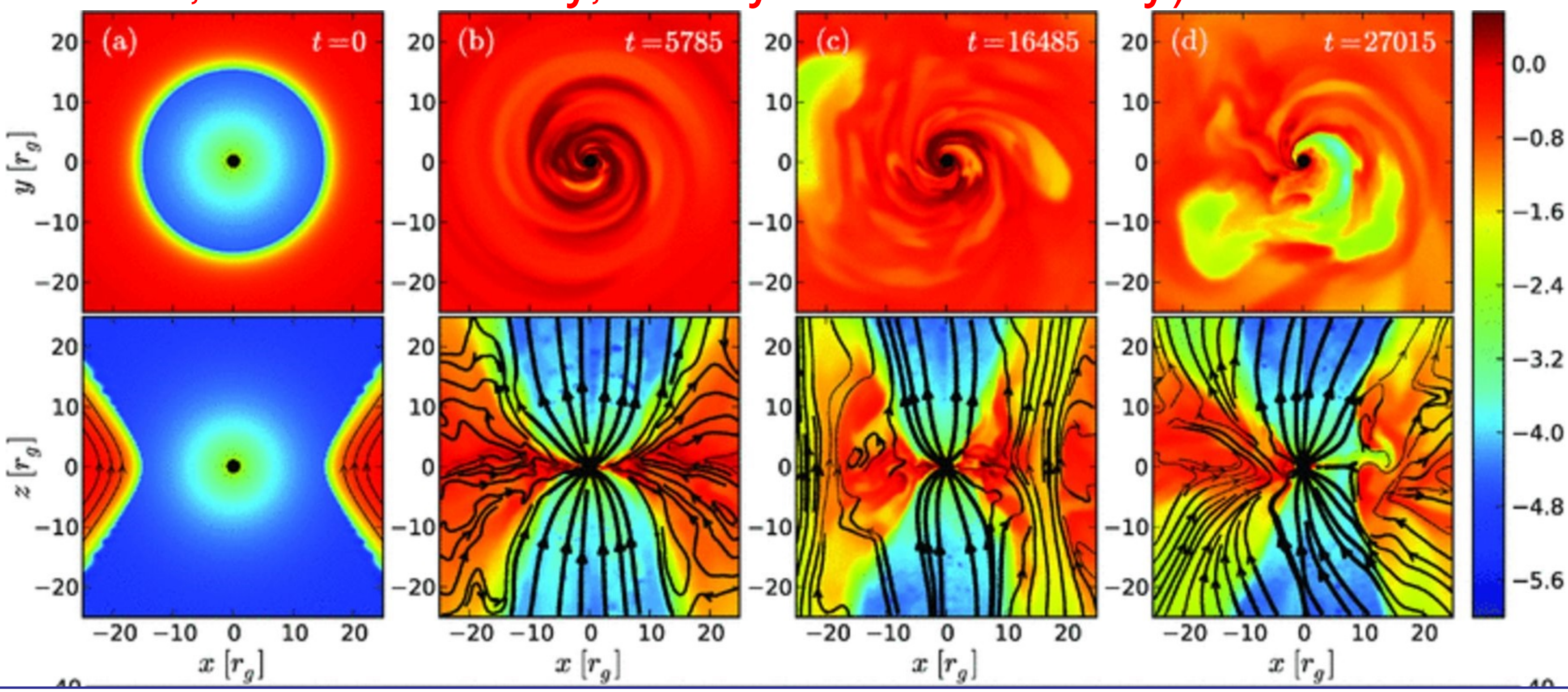

- our approach:

- focus on the propagation phase
- assume cylindrical unperturbed jet
- linear (normal mode) analysis
- A similar analysis from Hardee 2007 for $B_\phi = 0$ and Bodo+2013 for $V_\phi = 0$

try to understand how a jet is transformed to stable configuration

first step to find the dependence of the growth rate on various jet parameters

Unperturbed flow

Unperturbed relativistic cylindrical jet

helical, axisymmetric, cylindrically symmetric and steady flow

$$\boldsymbol{V}_0 = V_{0z}(r)\hat{z} + V_{0\phi}(r)\hat{\phi}\,, \quad \gamma_0 = \gamma_0(r) = (1 - V_{0z}^2 - V_{0\phi}^2)^{-1/2}\,,$$

$$\boldsymbol{B}_0 = B_{0z}(r)\hat{z} + B_{0\phi}(r)\hat{\phi}\,, \quad \boldsymbol{E}_0 = (V_{0z}B_{0\phi} - V_{0\phi}B_{0z})\hat{r}\,,$$

$$\rho_{00} = \rho_{00}(r)\,, \quad \xi_0 = \xi_0(r)\,, \quad \Pi_0 = \frac{\Gamma - 1}{\Gamma}(\xi_0 - 1)\,\rho_{00} + \frac{B_0^2 - E_0^2}{2}\,.$$

Equilibrium condition $\dfrac{B_{0\phi}^2 - E_0^2}{r} - \xi_0\rho_{00}\dfrac{\gamma_0^2 V_{0\phi}^2}{r} + \dfrac{d\Pi_0}{dr} = 0\,.$

Linearized equations

$$Q(r\,,z\,,\phi\,,t) = Q_0(r) + Q_1(r)\exp\left[i(m\phi + kz - \omega t)\right]$$

$$\left(\begin{array}{c} 10 \times 12 \text{ array} \\ \text{function of } r\,,\omega\,,k \end{array}\right) \begin{pmatrix} \gamma_1 \\ \rho_{01} \\ B_{1z} \\ B_{1\phi} \\ iB_{1r} \\ \xi_1 \\ V_{1z} \\ V_{1\phi} \\ d\,(irV_{1r})/dr \\ d\Pi_1/dr \\ irV_{1r} \\ \Pi_1 \end{pmatrix} = 0$$

reduces to (4 equations in real space)

$$\frac{d}{dr}\left(\begin{array}{c} y_1 \\ y_2 \end{array}\right) + \frac{1}{\mathcal{D}}\left(\begin{array}{cc} \mathcal{F}_{11} & \mathcal{F}_{12} \\ \mathcal{F}_{21} & \mathcal{F}_{22} \end{array}\right)\left(\begin{array}{c} y_1 \\ y_2 \end{array}\right) = 0\,,$$

where the (complex) unknowns are

$$y_1 = i\frac{rV_{1r}}{\omega_0}\,, \qquad y_2 = \Pi_1 + \frac{y_1}{r}\frac{d\Pi_0}{dr}$$

($\mathcal{D}\,, \mathcal{F}_{ij}$ are determinants of 10×10 arrays).

Equivalently

$$y_2'' + \left[\frac{\mathcal{F}_{11}+\mathcal{F}_{22}}{\mathcal{D}} + \frac{\mathcal{F}_{21}}{\mathcal{D}}\left(\frac{\mathcal{D}}{\mathcal{F}_{21}}\right)'\right] y_2' + \left[\frac{\mathcal{F}_{11}\mathcal{F}_{22}-\mathcal{F}_{12}\mathcal{F}_{21}}{\mathcal{D}^2} + \frac{\mathcal{F}_{21}}{\mathcal{D}}\left(\frac{\mathcal{F}_{22}}{\mathcal{F}_{21}}\right)'\right] y_2 = 0\,,$$

which for uniform flows with $V_{0\phi} = 0$, $B_{0\phi} = 0$, reduces to Bessel.

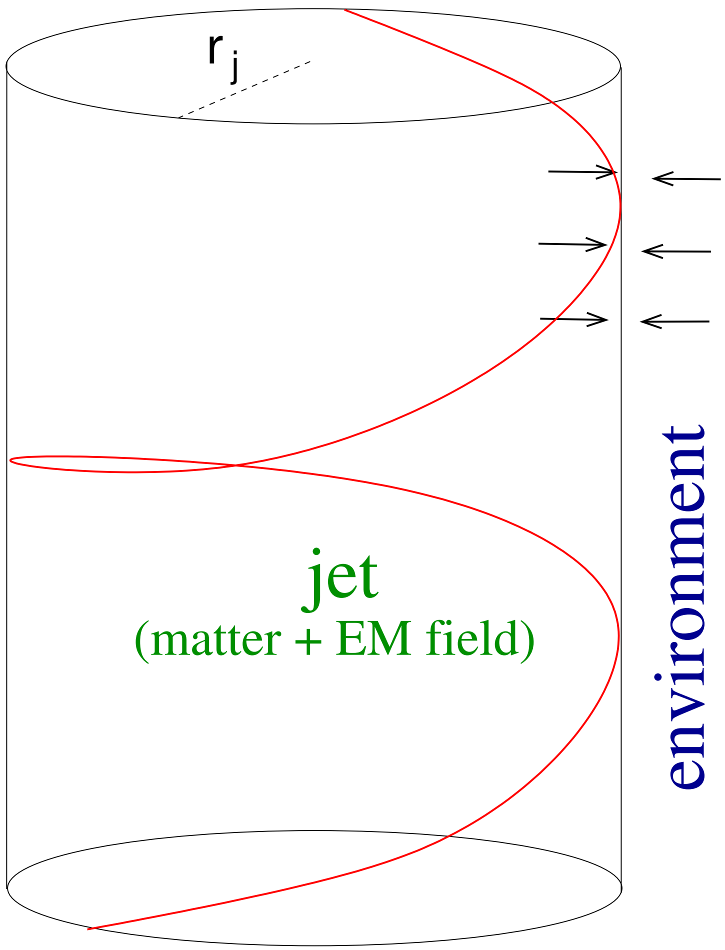

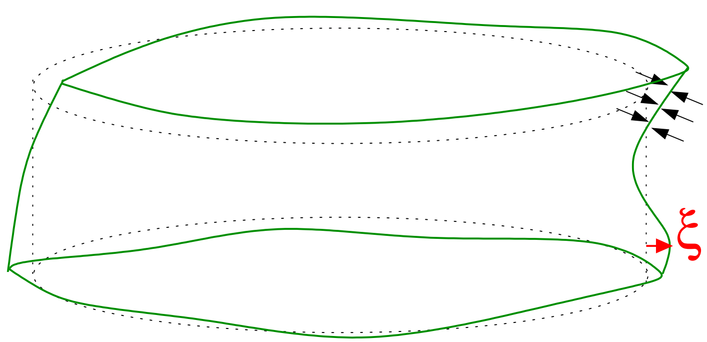

Eigenvalue problem

- solve the problem inside the jet (attention to regularity condition on the axis)

- similarly in the environment (solution vanishes at ∞)

- Match the solutions at r_j:

$[\![y_1]\!] = 0\,, [\![y_2]\!] = 0 \longrightarrow$ dispersion relation

$\star$ spatial approach: $\omega = \Re\omega$ and $\Re k = \Re k(\omega), \Im k = \Im k(\omega)$

$Q = Q_0(r) + Q_1(r) e^{-\Im k z} e^{i(m\phi + \Re k z - \omega t)}$

$\star$ temporal approach: $k = \Re k$ and $\Re\omega = \Re\omega(k), \Im\omega = \Im\omega(k)$

$Q = Q_0(r) + Q_1(r) e^{\Im\omega t} e^{i(m\phi + kz - \Re\omega t)}$

Unperturbed jet solutions

Try to mimic the Komissarov et al simulation results
(for AGN and GRB jets)

- cold, nonrotating jet

$$\boldsymbol{V}_0 = V_0(r)\hat{z}\,, \quad \gamma_0 = \gamma_0(r) = (1 - V_0^2)^{-1/2}\,,$$

$$\boldsymbol{B}_0 = B_{0z}(r)\hat{z} + B_{0\phi}(r)\hat{\phi}\,, \quad \boldsymbol{E}_0 = V_0 B_{0\phi}\hat{r}\,,$$
$$\rho_{00} = \rho_{00}(r)\,, \quad \xi_0 = 1\,.$$

- Equilibrium condition (“force-free”)

$$\frac{B_{0\phi}^2/\gamma_0^2}{r} + \frac{d}{dr}\left(\frac{B_{0z}^2 + B_{0\phi}^2/\gamma_0^2}{2}\right) = 0\,,$$

relates B_{0z} with $B_{0\phi}/\gamma_0$.

A cold, nonrotating solution:

$$B_{0z} = \frac{B_j}{\left[1+(r/r_0)^2\right]^{\zeta}}\,, \quad B_{0\phi} = -\gamma_0 B_{0z}\sqrt{\frac{\left[1+(r/r_0)^2\right]^{2\zeta} - 1 - 2\zeta(r/r_0)^2}{(2\zeta-1)(r/r_0)^2}}\,.$$

$r_0\,, \zeta$ free parameters, $\gamma_0\,, \rho_{00}$ free functions.

- choice of ζ:

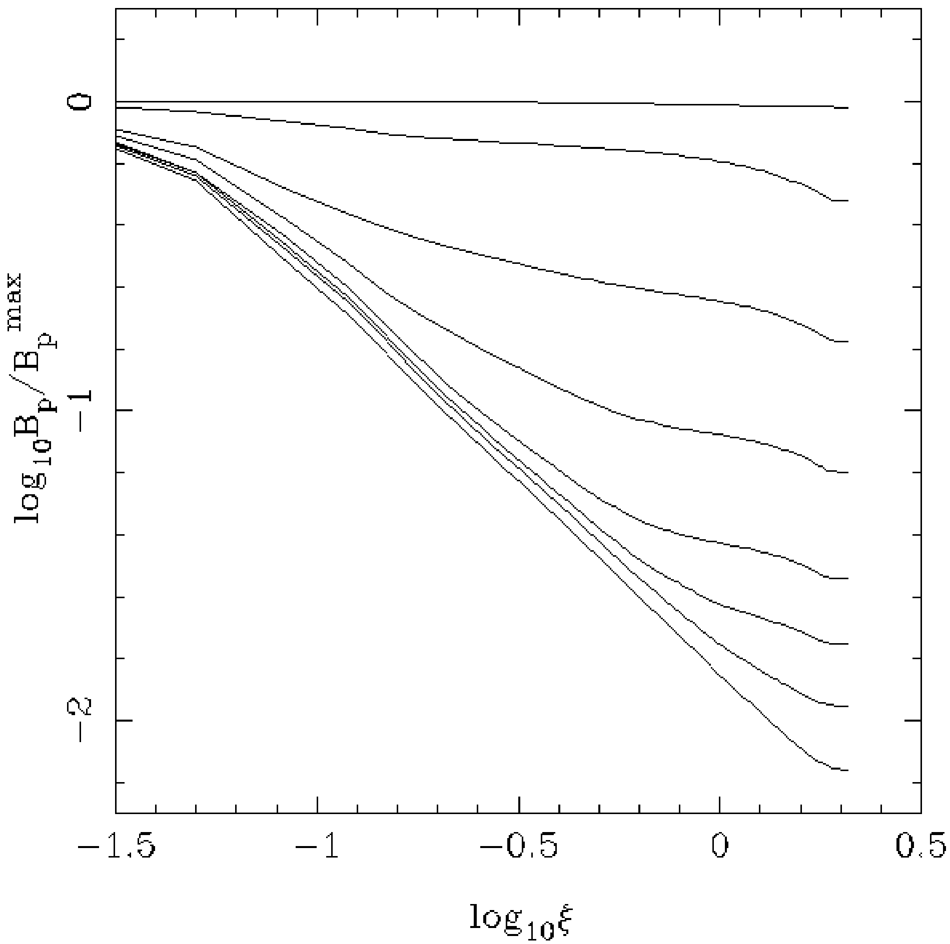

$B_{0z} \propto r^{-1.2}$

$\zeta = 0.6$

Formation of core crucial for the acceleration.

The bunching function $\mathcal{S} \equiv \dfrac{\overbrace{\pi r^2}^{S} B_{0z}}{\int_0^r B_{0z} \underbrace{2\pi r dr}_{dS}}$ is related to the acceleration efficiency $\sigma = \dfrac{1}{\frac{\mathcal{S}_f}{\mathcal{S}} - 1}$, where $\mathcal{S}_f$ integral of motion ~ 0.9.

Since $\mathcal{S} \approx 1 - \zeta$ we get $\sigma = \dfrac{1-\zeta}{\zeta - 0.1} = 0.8$.

- choice of $\gamma_0(r)$:

From Ferraro's law $V_{0\phi} = r\Omega + V_{0z}B_{0\phi}/B_{0z}$, where Ω integral of motion, we get $-B_{0\phi}/B_{0z} \approx r\Omega/V_{0z}$. Using the given expressions of $B_{0\phi}/\gamma_0$, B_{0z}, $\gamma_0 = \sqrt{1 + r_0^2\Omega^2 \frac{(2\zeta-1)(r/r_0)^4}{\left[1+(r/r_0)^2\right]^{2\zeta}-1-2\zeta(r/r_0)^2}}$.

On the axis $\left.\dfrac{\gamma_0 V_0}{\Omega}\right|_{axis} = \dfrac{r_0}{\sqrt{\zeta}}$ (gives $\Omega|_{axis}$ for given γ_{0axis}, r_0).

The choice of r_0, $\Omega(r)$ controls the pitch $B_{0\phi}/(rB_{0z})$, and the values of γ_0 on the axis and the jet surface.

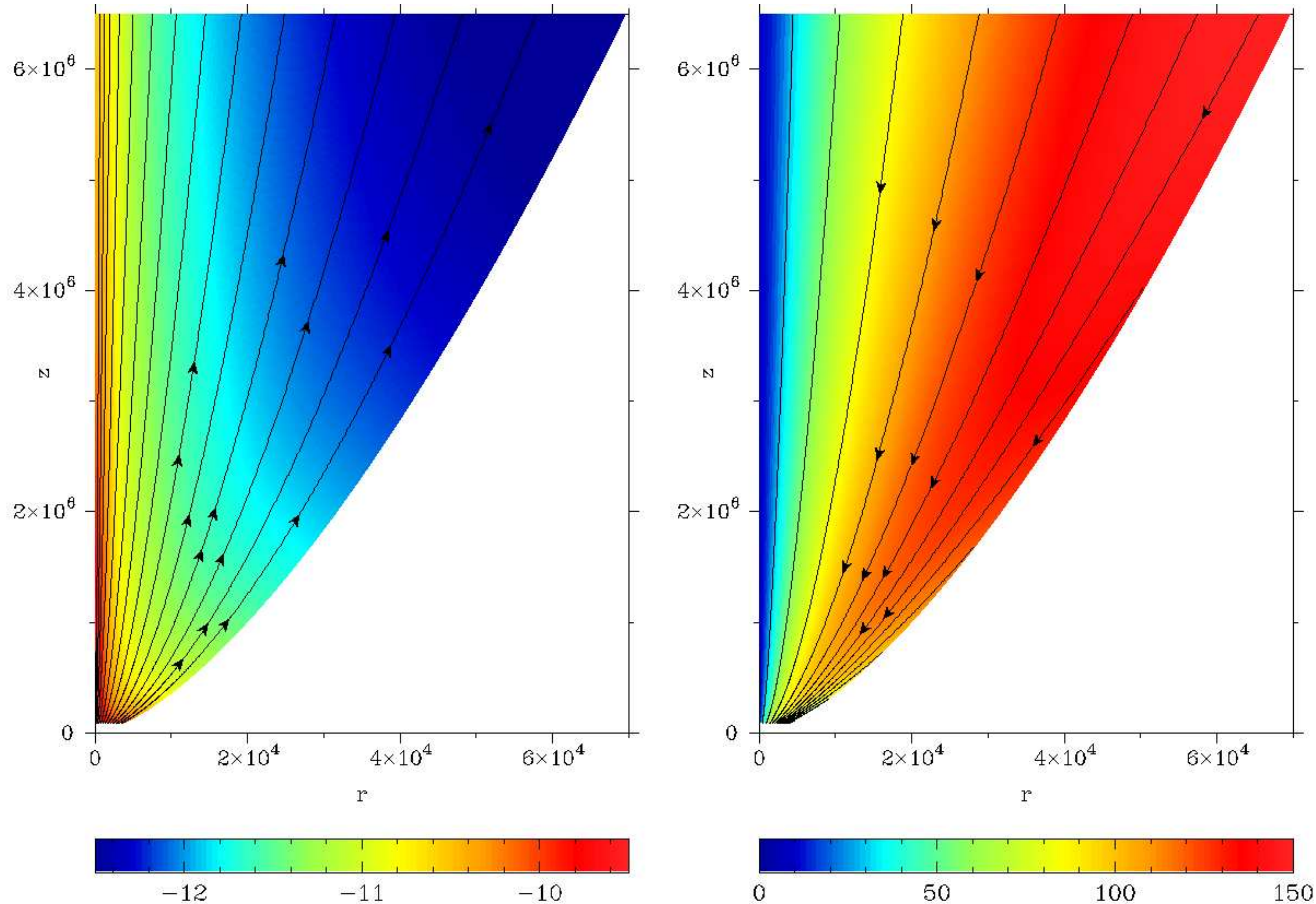

left: density/field lines, right: Lorentz factor/current lines (jet boundary $z \propto r^{1.5}$)
Uniform rotation $\rightarrow \gamma$ increases with r

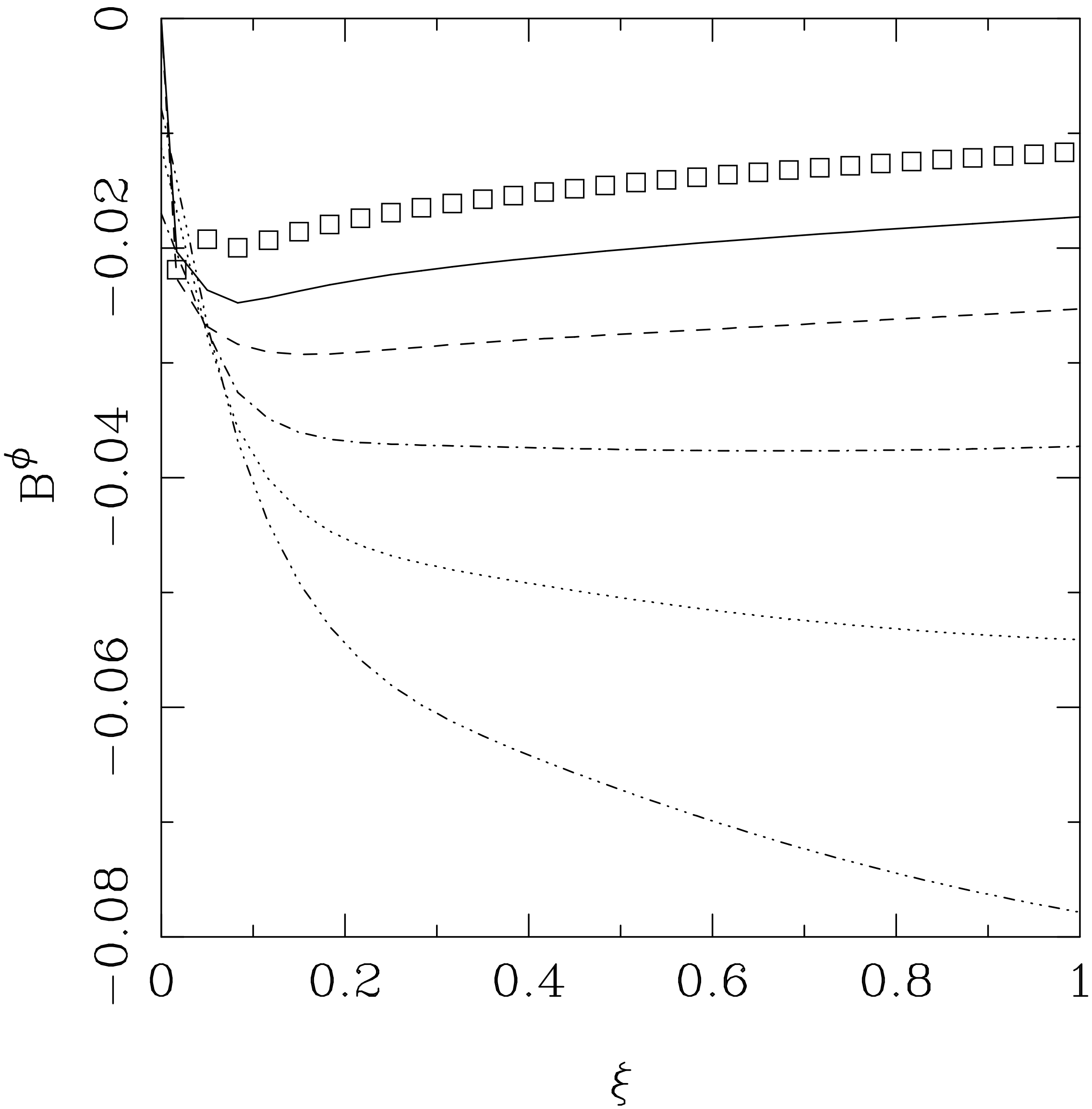
0
−0.02
−0.04
−0.06
−0.08
B^ϕ
0
0.2
0.4
0.6
0.8
1
ξ

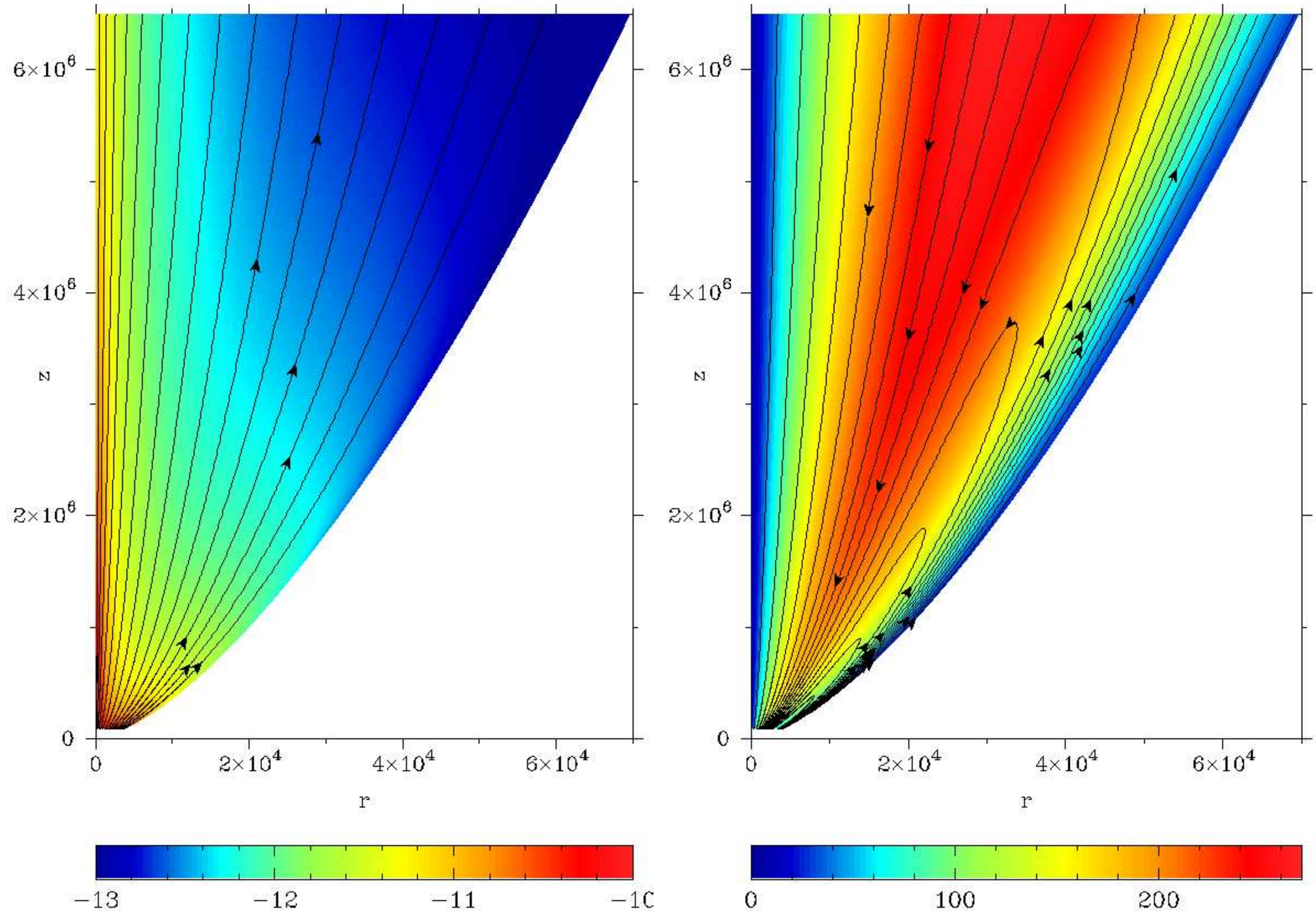

Differential rotation $\rightarrow$ slow envelope and faster decrease of B_ϕ

- choice of $\rho_{00}(r)$:

This comes from the mass-to-magnetic flux ratio integral $\frac{\gamma_0 \rho_{00} V_0}{B_{0z}}$, which is assumed constant in the simulations. So $\rho_{00} \propto B_{0z}/\gamma_0$.

The constant of proportionality from the value of $\sigma = \left.\frac{B_{0\phi}^2/\gamma_0^2}{\rho_{00}}\right|_{r=r_j}$.

- external medium:

uniform, static, with zero $B_{0\phi}$ and $V_{0\phi} \rightarrow$ Bessel.
In all the following a thermal pressure is assumed, $\xi_e = 1.01$ (the value of ξ_e controls the density ratio).
A cold, magnetized environment gives approximatelly same results.

Ω=const, $-B_\phi/B_z$=31 r /r$_j$

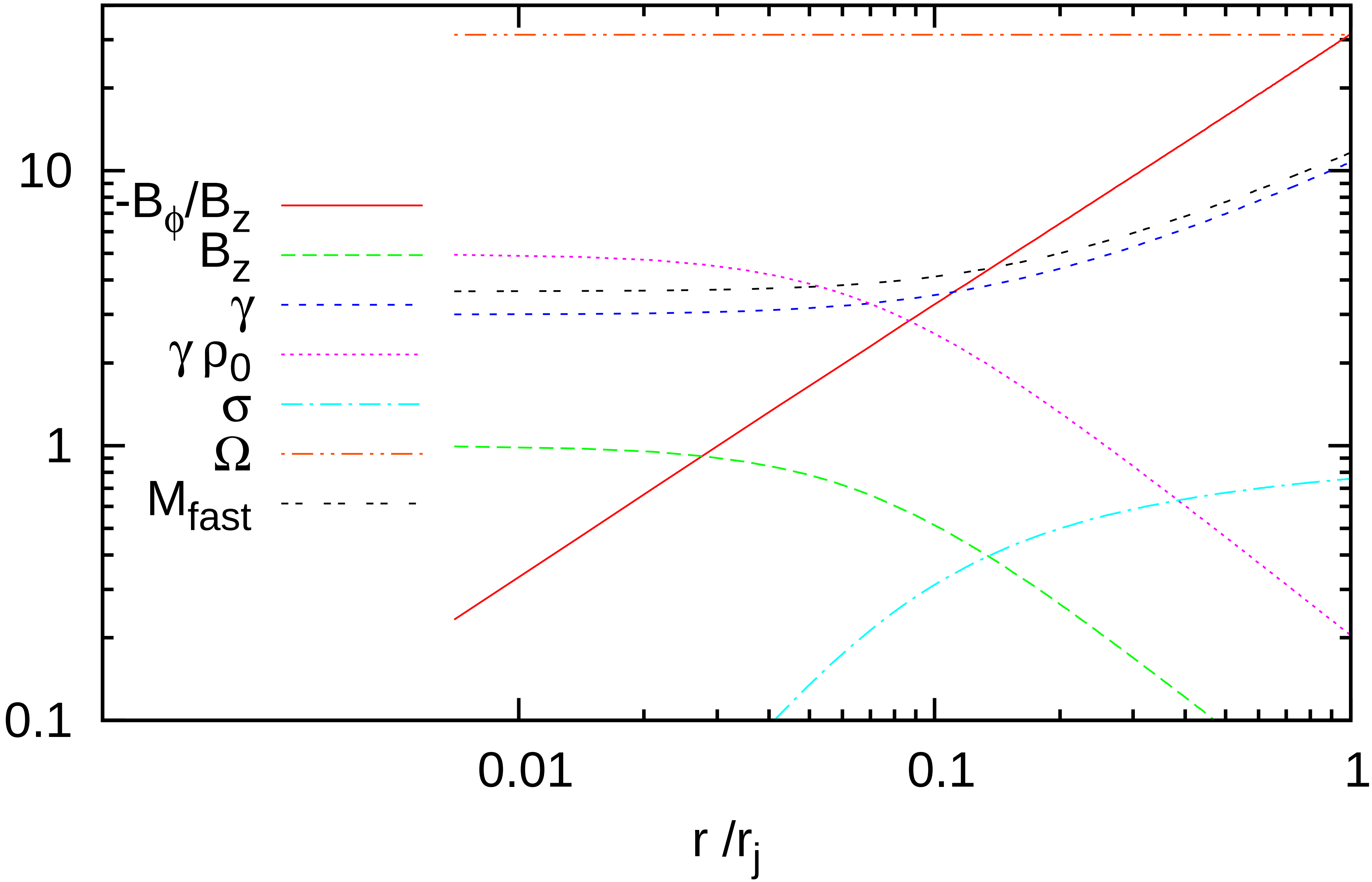

A “fundamental” and multiple ”reflective” modes

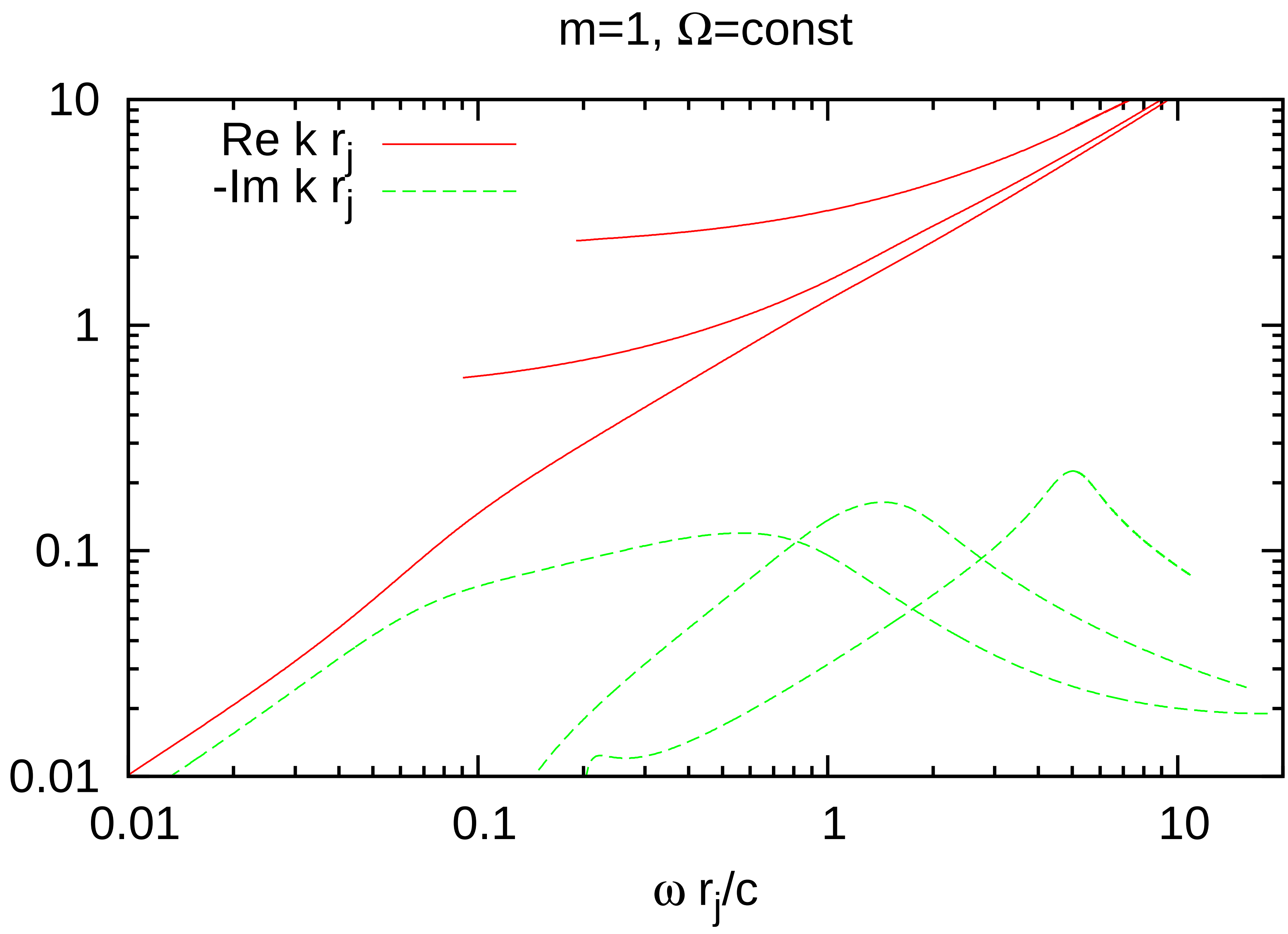

$Q = Q_0(r) + Q_1(r)e^{-\Im kz}e^{i(m\phi + \Re kz - \omega t)}$

growth length $= 1/(-\Im k) \sim r_j/0.2 = 5r_j$

nonlinear effects important after a few $10r_j$

growth time $\approx$ growth length ($c = 1$)

growth rate $\approx -\Im k \sim 0.2/r_j$

in rough agreement with nonrelativistic linear studies which predict growth rates in comoving frame $\Gamma_{\rm co} \sim \dfrac{v_A}{10r_0}$ (Appl et al)

in the lab frame $\Gamma = \dfrac{\Gamma_{\rm co}}{<\gamma>} \approx 0.2/r_j$

($v_A = \sqrt{\frac{\sigma}{\sigma+1}} \sim \frac{2}{3}, \quad r_0 = 0.1r_j, \quad <\gamma> \sim 5$)

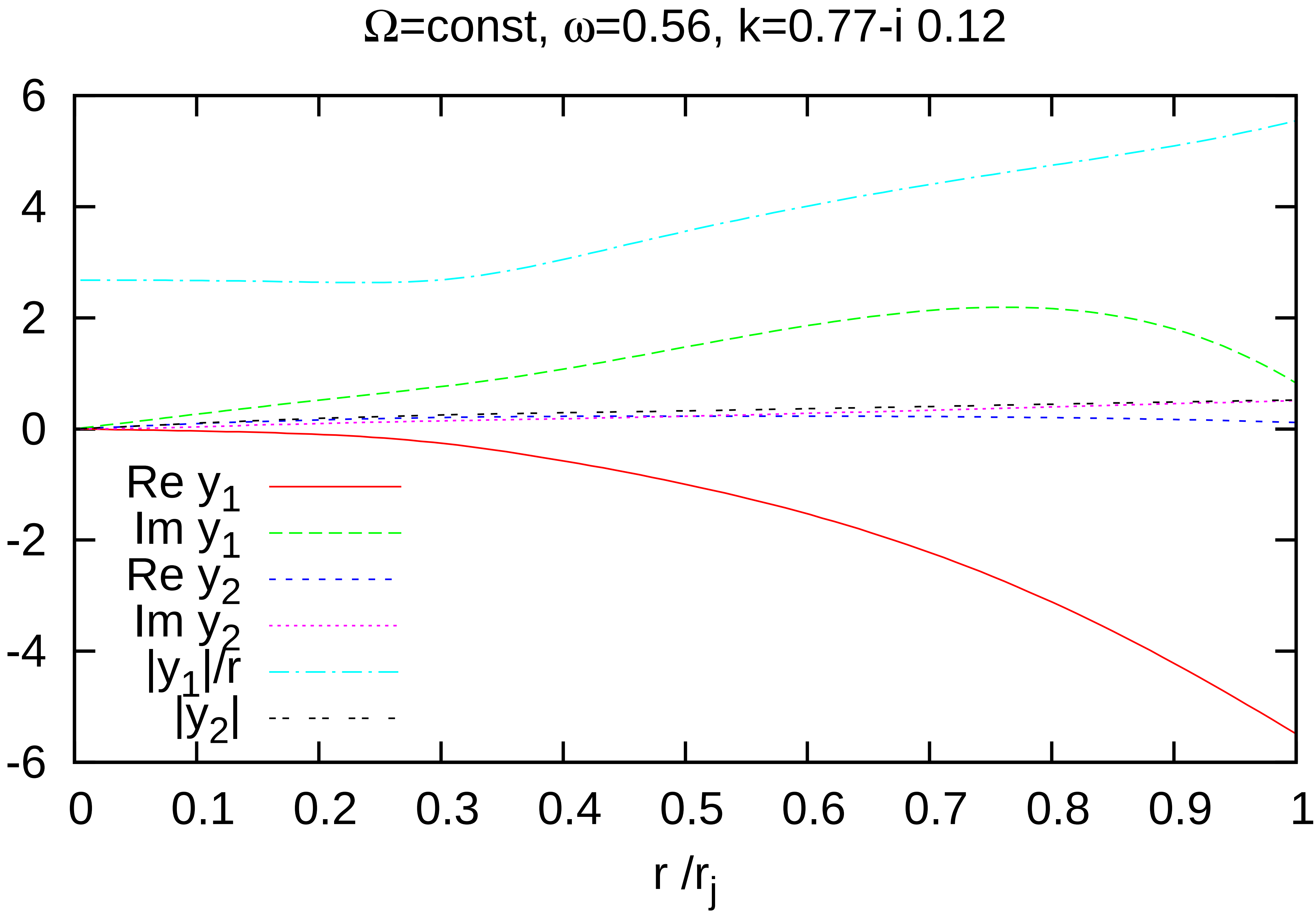
Ω=const, ω=0.56, k=0.77-i 0.12
6
4
2
0
-2
-4
-6
0
0.1
0.2
0.3
0.4
0.5
0.6
0.7
0.8
0.9
1
r /r_j
Re y_1
Im y_1
Re y_2
Im y_2
|y_1|/r
|y_2|

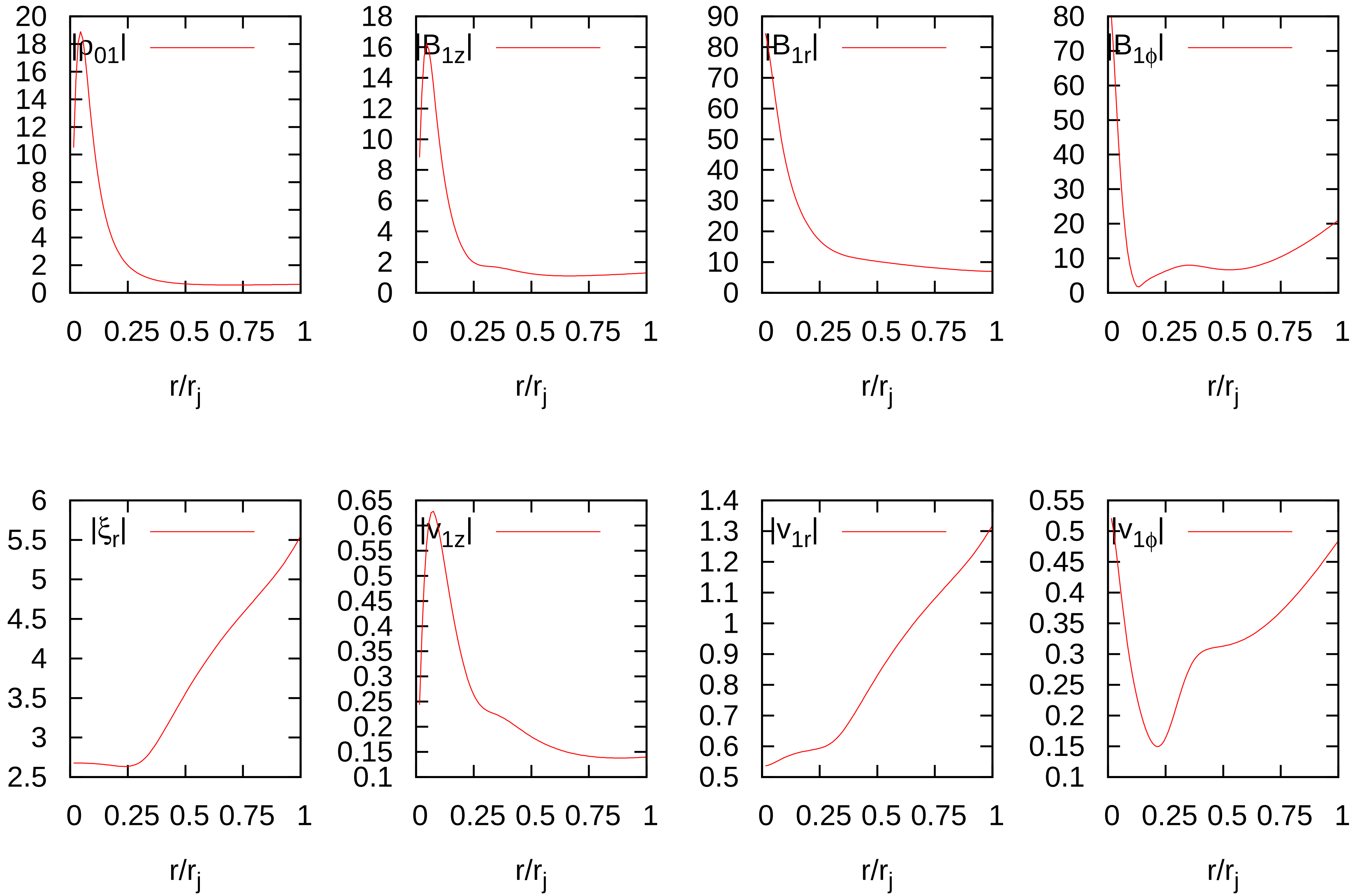

|ρ01|
|B1z|
|B1r|
|B1φ|
|ξr|
|v1z|
|v1r|
|v1φ|
r/rj

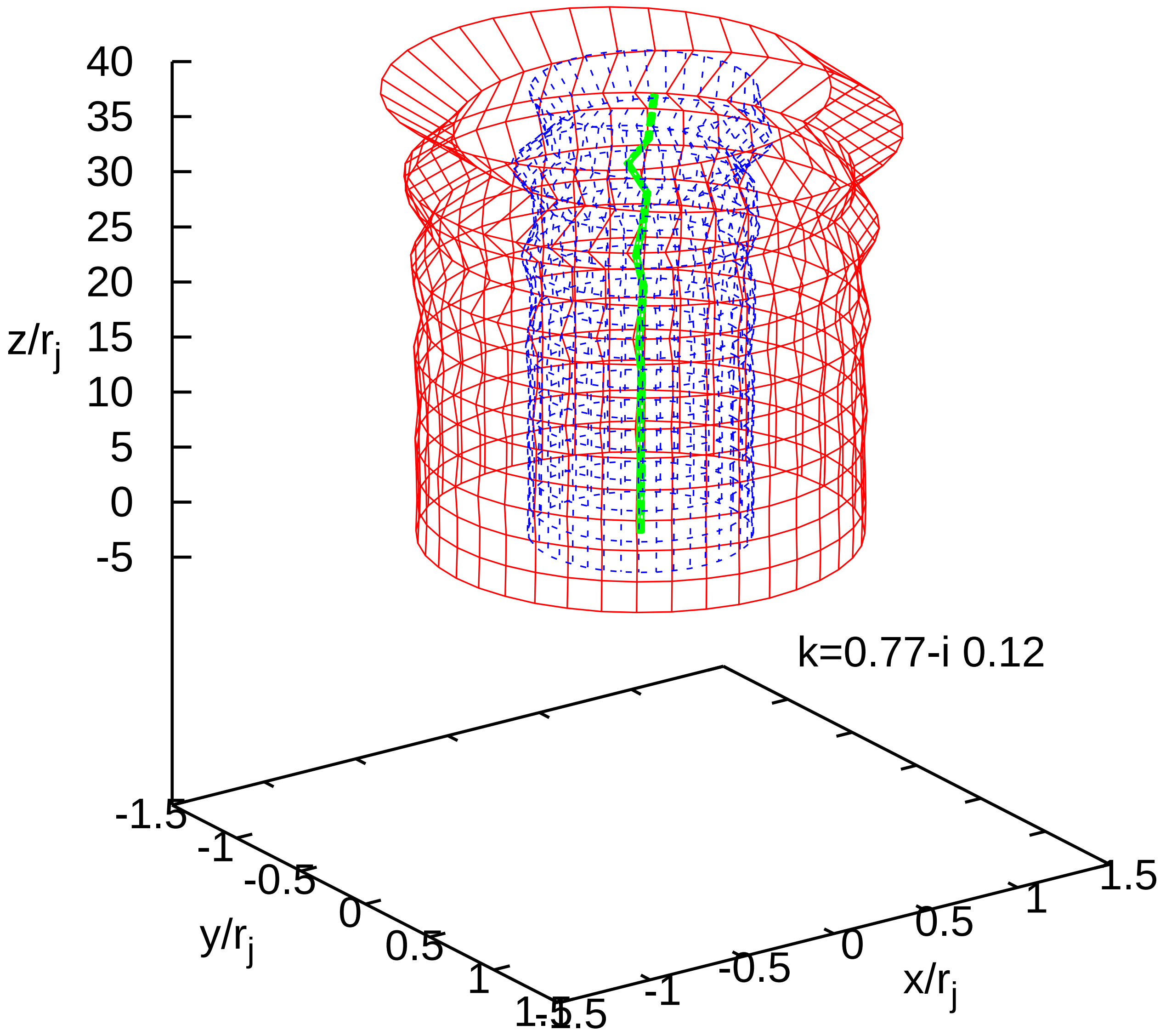
40
35
30
25
20
15
10
5
0
-5
z/r_j
k=0.77-i 0.12
-1.5
-1
-0.5
0
0.5
1
1.5
y/r_j
-1.5
-1
-0.5
0
0.5
1
1.5
x/r_j

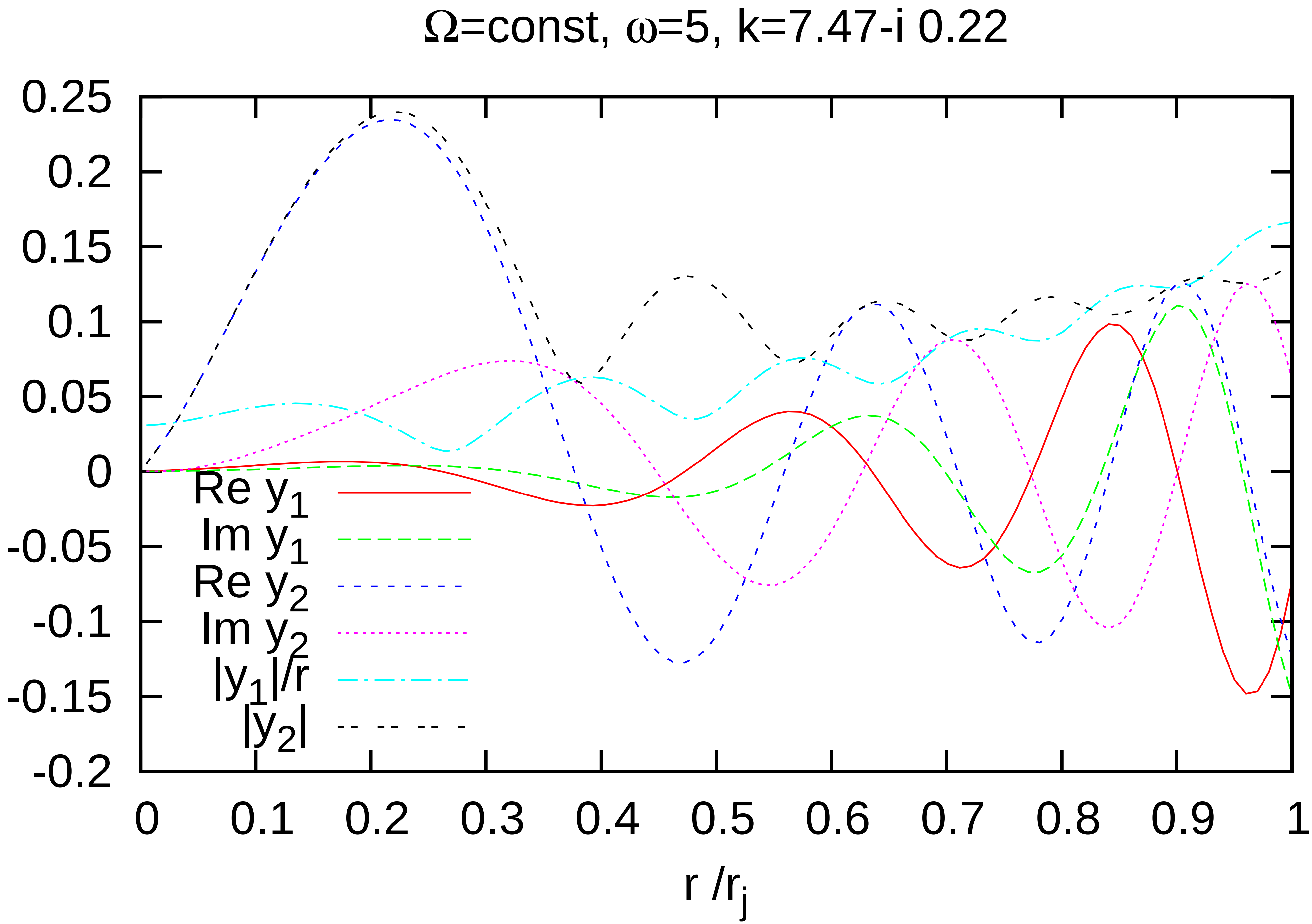
Ω=const, ω=5, k=7.47-i 0.22
0.25
0.2
0.15
0.1
0.05
0
-0.05
-0.1
-0.15
-0.2
0
0.1
0.2
0.3
0.4
0.5
0.6
0.7
0.8
0.9
1
r /r$_j$
Re y_1
Im y_1
Re y_2
Im y_2
$|y_1|/r$
$|y_2|$

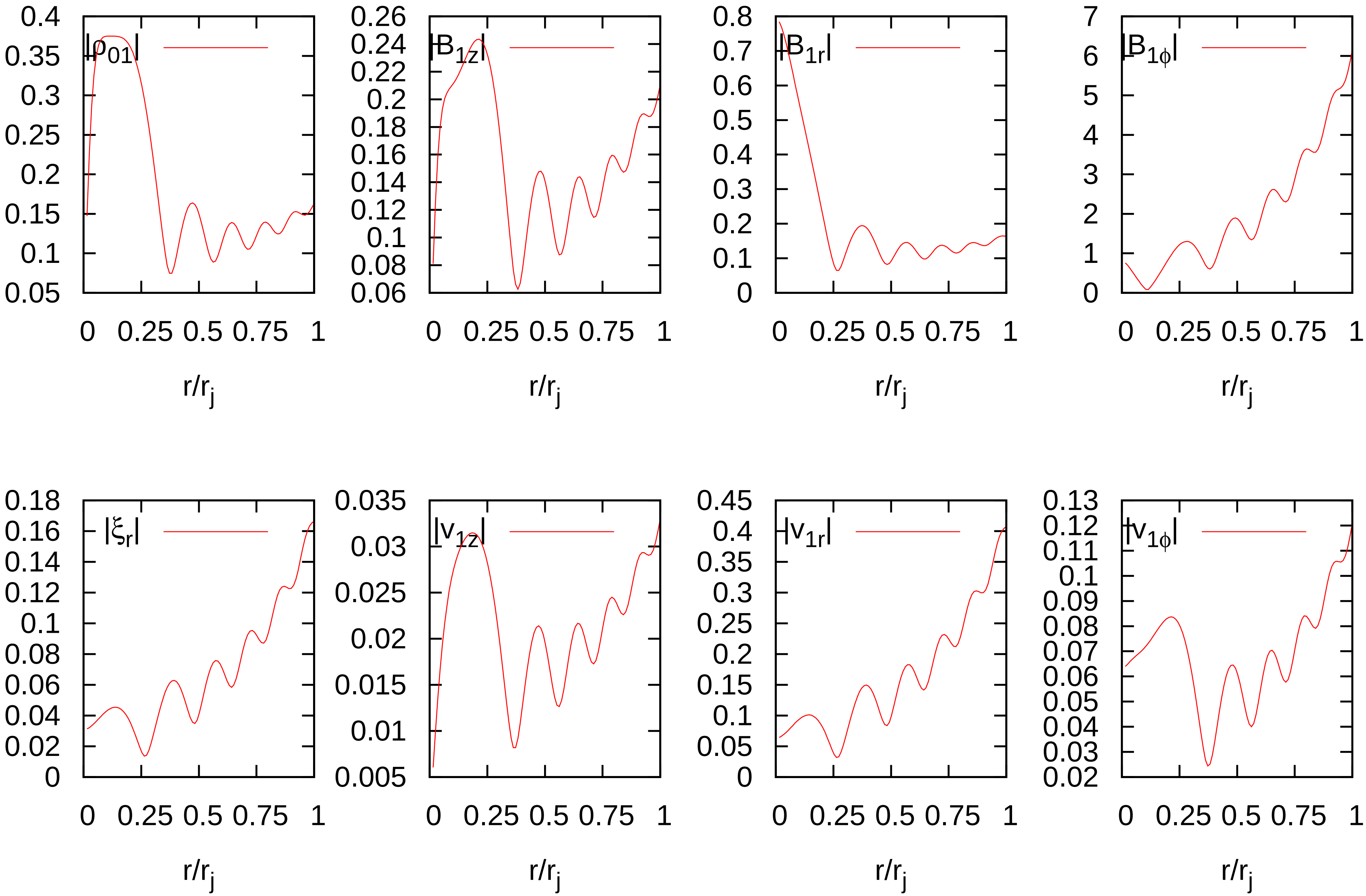
|ρ01|
|B1z|
|B1r|
|B1ϕ|
|ξr|
|v1z|
|v1r|
|v1ϕ|
r/rj

Ω=const, $-B_\phi/B_z$=22 r /r$_j$

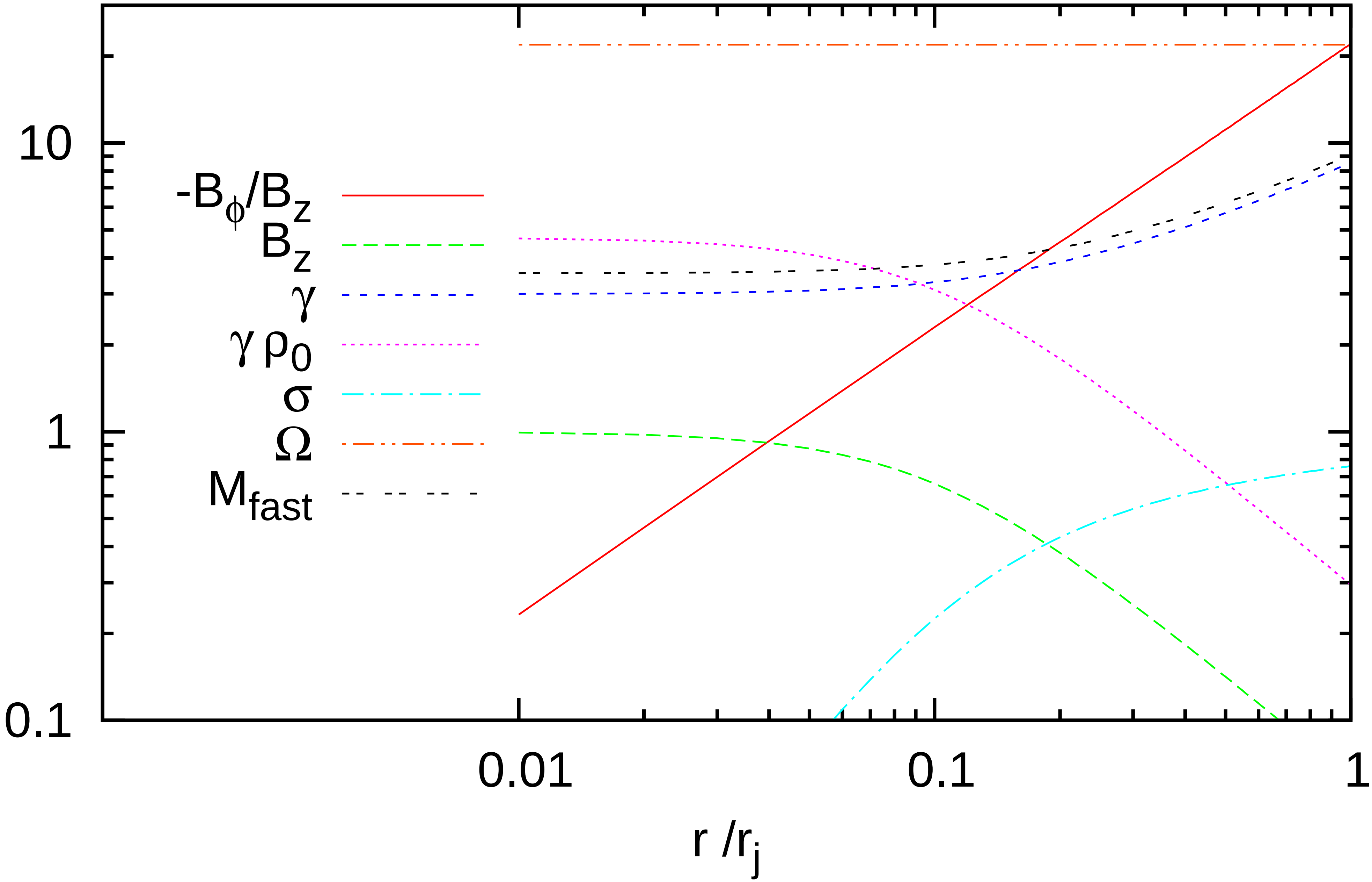

m=1, Ω=const

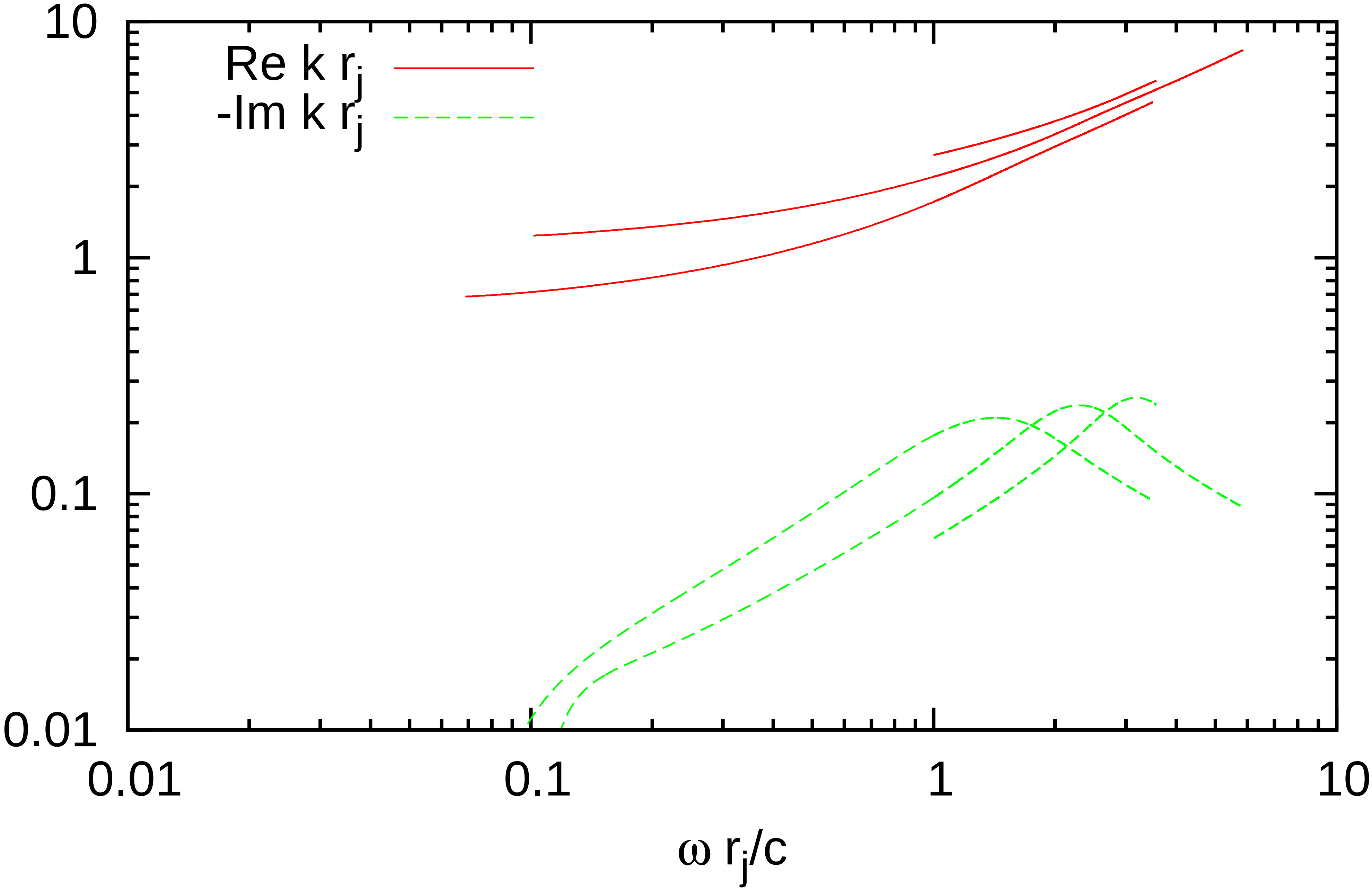

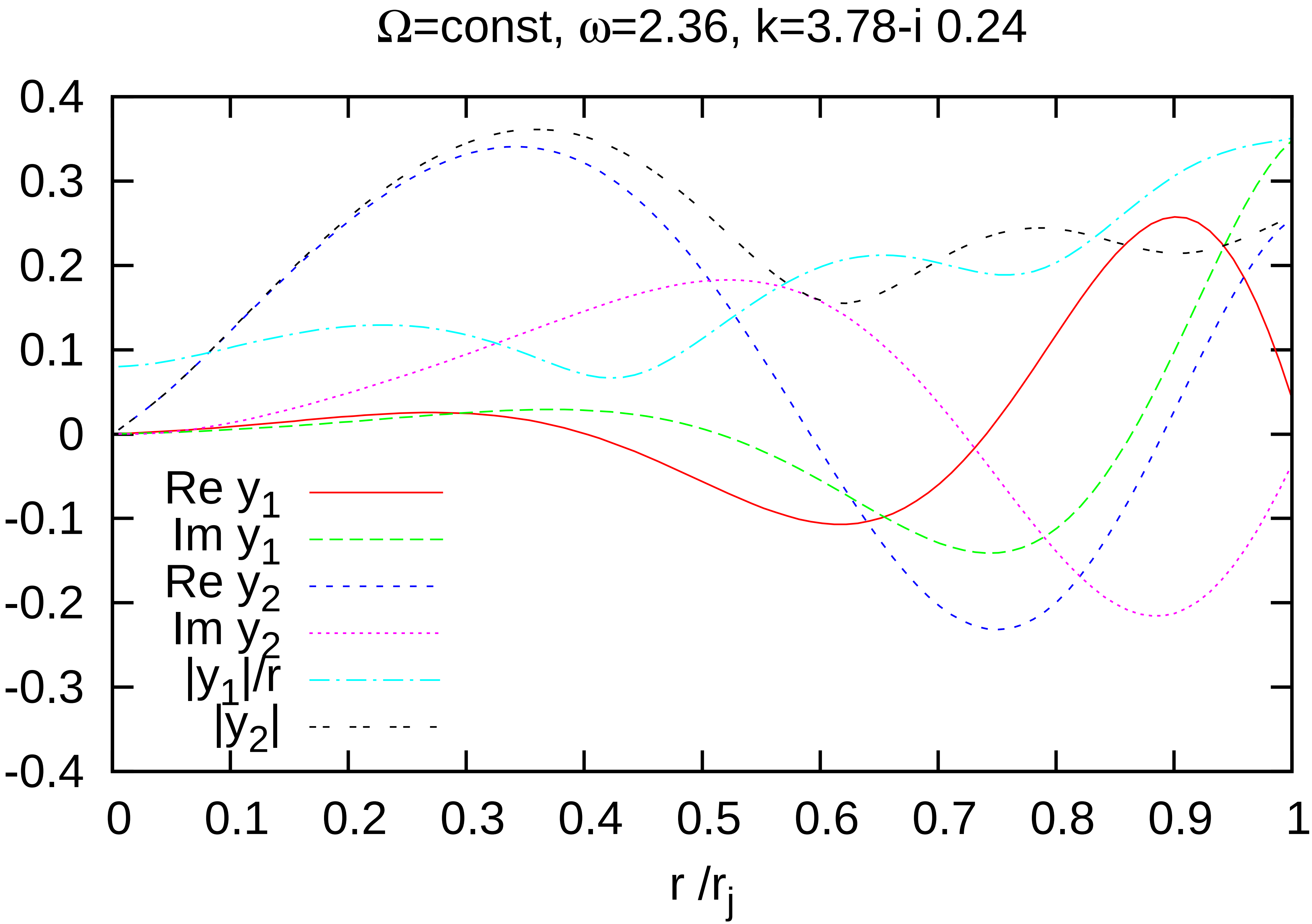
Ω=const, ω=2.36, k=3.78-i 0.24
0.4
0.3
0.2
0.1
0
-0.1
-0.2
-0.3
-0.4
0
0.1
0.2
0.3
0.4
0.5
0.6
0.7
0.8
0.9
1
r /r_j
Re y_1
Im y_1
Re y_2
Im y_2
|y_1|/r
|y_2|

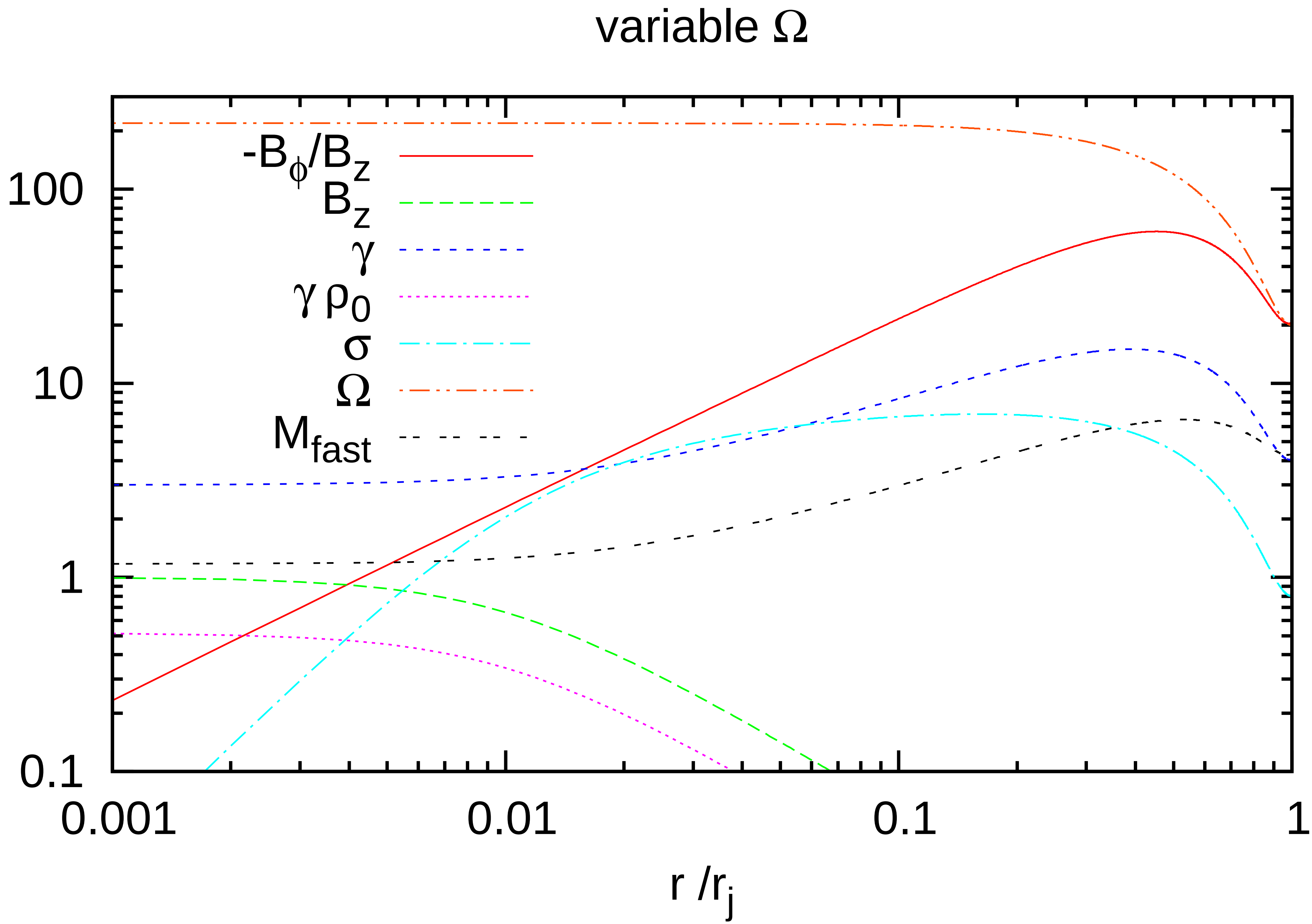

variable Ω
$-B_\phi/B_z$
B_z
γ
$\gamma\,\rho_0$
σ
Ω
M_{fast}
100
10
1
0.1
0.001
0.01
0.1
1
$r\,/r_j$

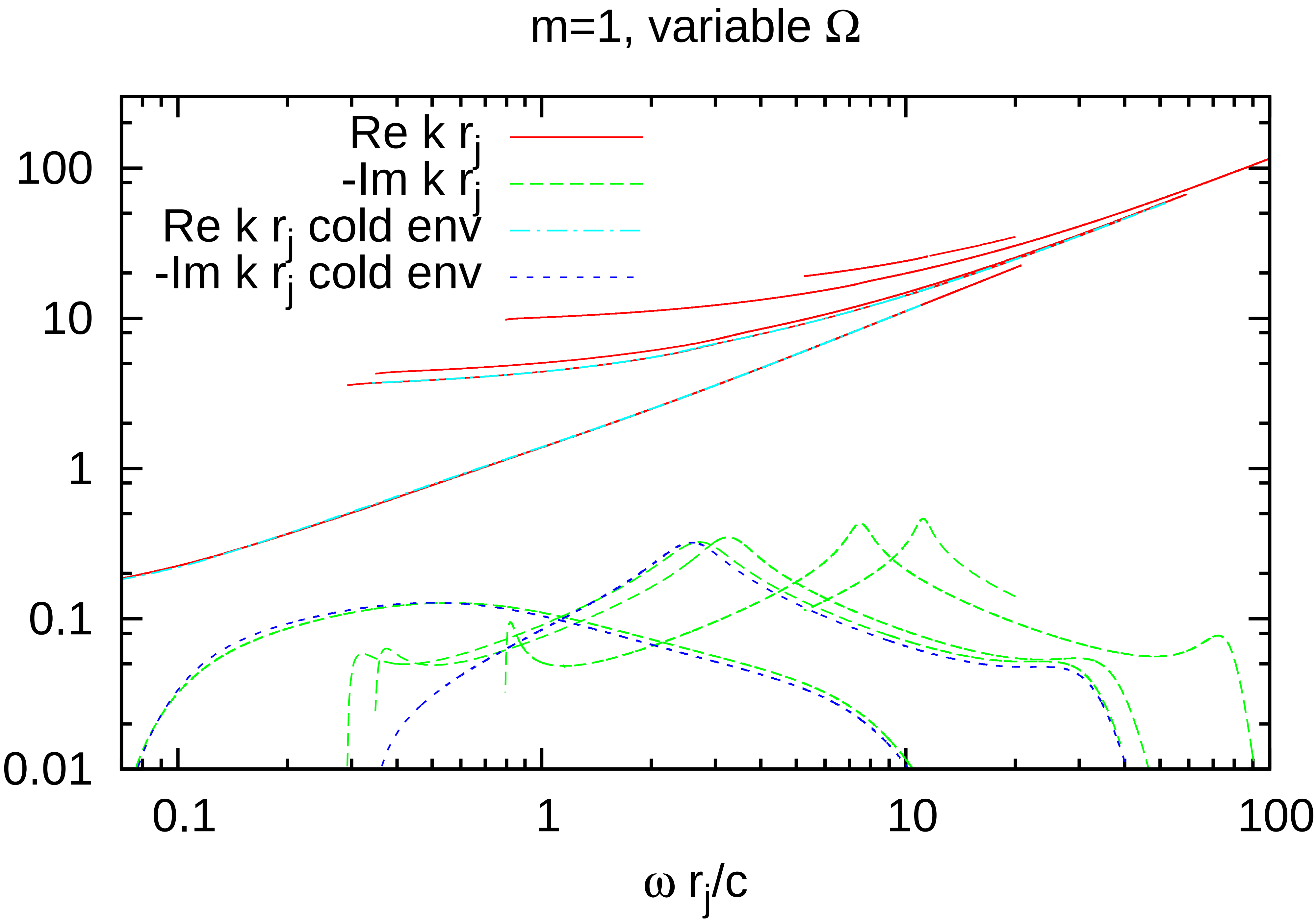
m=1, variable Ω
Re k r_j
-Im k r_j
Re k r_j cold env
-Im k r_j cold env
100
10
1
0.1
0.01
0.1
1
10
100
ω r_j/c

variable Ω, ω=0.55, k=0.84-i 0.13

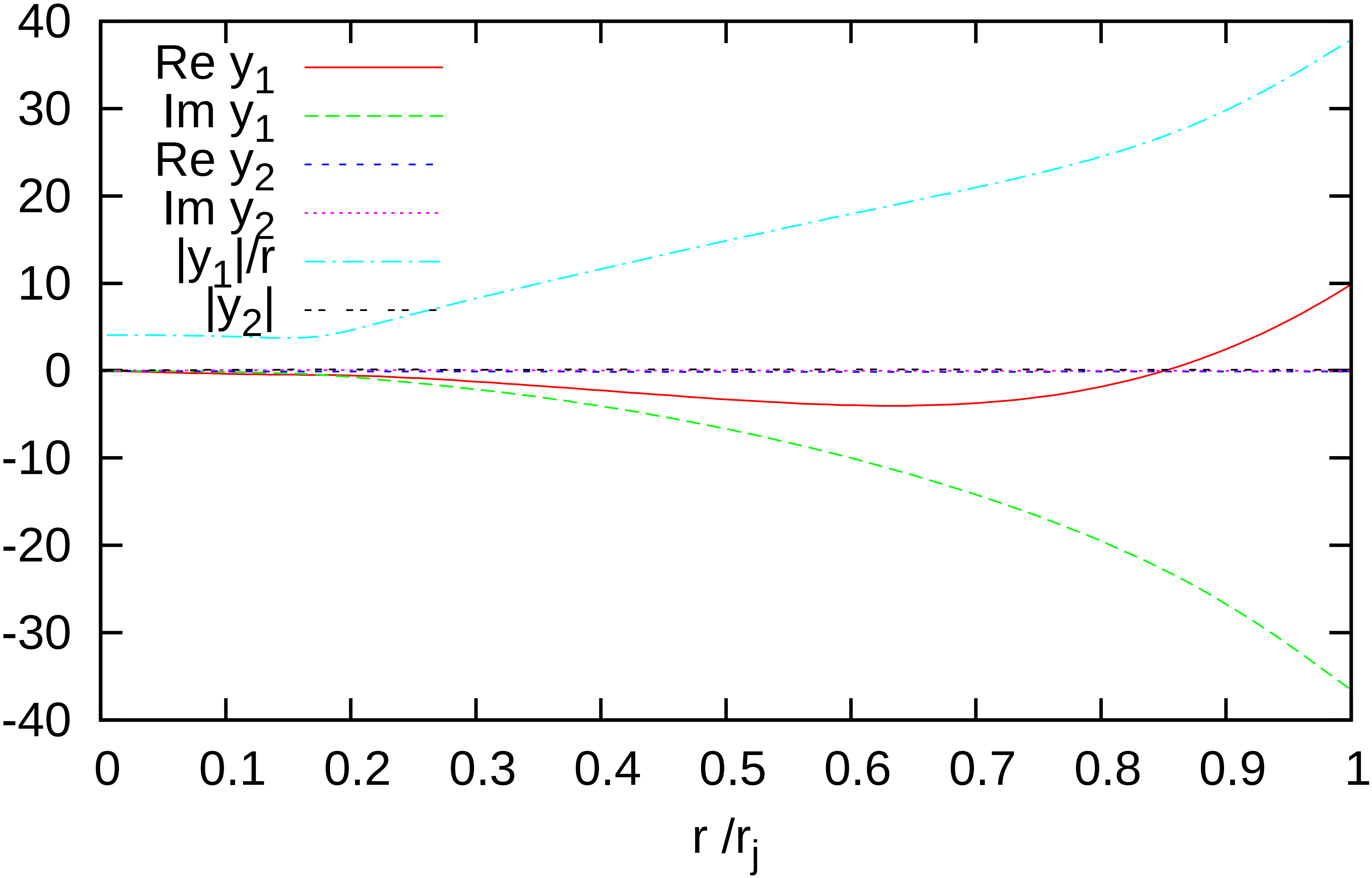

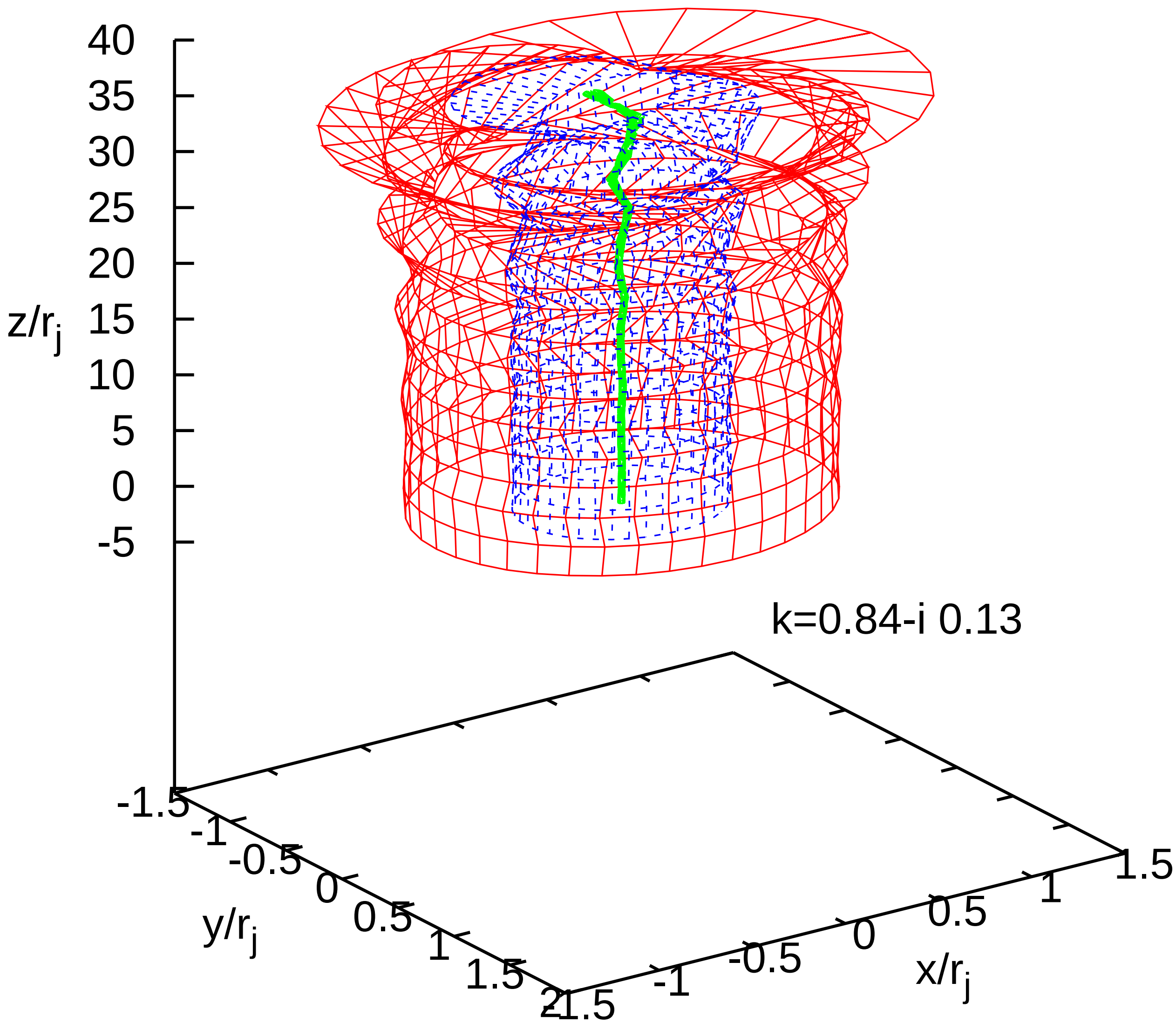
40
35
30
25
20
15
10
5
0
-5
z/r_j
k=0.84-i 0.13
-1.5
-1
-0.5
0
0.5
1
1.5
2
y/r_j
-1.5
-1
-0.5
0
0.5
1
1.5
x/r_j

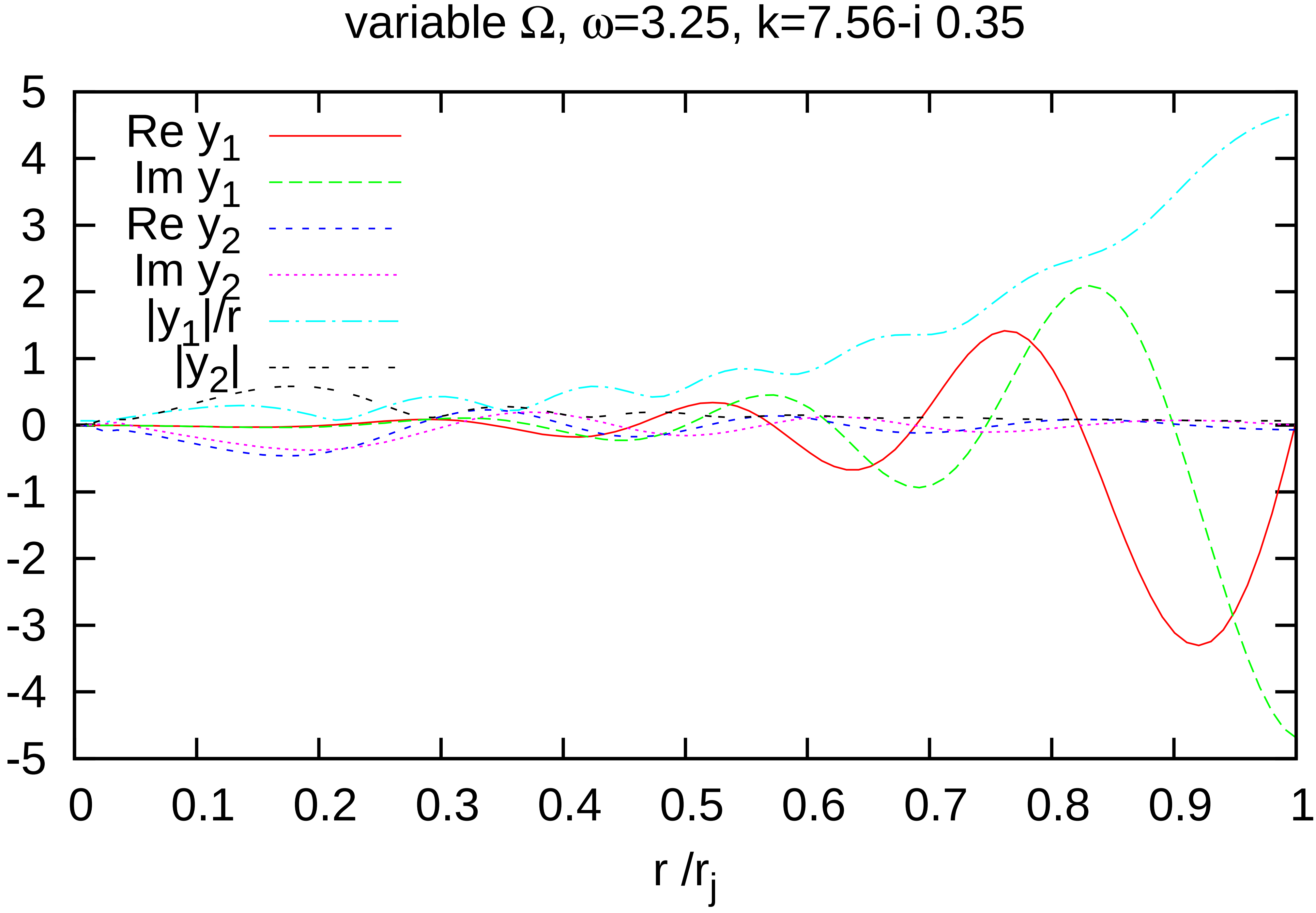

variable Ω, ω=3.25, k=7.56-i 0.35
Re y_1
Im y_1
Re y_2
Im y_2
$|y_1|/r$
$|y_2|$
5
4
3
2
1
0
-1
-2
-3
-4
-5
0
0.1
0.2
0.3
0.4
0.5
0.6
0.7
0.8
0.9
1
r/r_j

Summary – Discussion – Next steps

⋆ Kink instability in principle is in action (similar to nonrelativistic)

⋆ Low $(|B_\phi|/B_z)_{\rm co}$, low σ, high γ, stabilize

⋆ The flow is significantly disrupted after a few $10 r_j$
(nonlinear evolution through simulations only)

- Explore the parameter space for kink and other modes

- colder/moving environment? other jet equilibrium models? role of velocity shear?

- use the eigenstates as initial conditions in numerical studies – how the jet is transformed to a stable configuration?

- during acceleration? effect of poloidal curvature and lateral expansion of jet? (causality)